

We are IntechOpen, the world's leading publisher of Open Access books Built by scientists, for scientists

6,900

Open access books available

186,000

International authors and editors

200M

Downloads

Our authors are among the

154

Countries delivered to

TOP 1%

most cited scientists

12.2%

Contributors from top 500 universities



WEB OF SCIENCE™

Selection of our books indexed in the Book Citation Index
in Web of Science™ Core Collection (BKCI)

Interested in publishing with us?
Contact book.department@intechopen.com

Numbers displayed above are based on latest data collected.
For more information visit www.intechopen.com



Superconductivity in Nanoscale Systems

Meenakshi Singh², Yi Sun¹ and Jian Wang^{1,2*}

¹*International Center for Quantum Materials & State Key Laboratory for Mesoscopic Physics, School of Physics, Peking University, Beijing,*

²*The Center for Nanoscale Science & Department of Physics, The Pennsylvania State University, University Park,*

¹*China*

²*USA*

1. Introduction

According to the BCS theory, charge transport in superconductors is carried out by paired electrons named 'Cooper pairs'. The distance between a pair of electrons is called the superconducting coherence length (ξ). If superconductivity is made possible by electrons 'holding hands' to form Cooper pairs, what happens to the superconductivity when one or more dimensions of the sample are smaller than the size of the cooper pair (ξ)? The answer to this question is of both fundamental interest and practical importance. The fundamental interest stems from the fact that in these reduced dimensionality systems, fluctuations play a very important role, even at low temperatures. In addition, because of the large surface to volume ratio, surface effects become important. Therefore, many novel phenomena not seen in bulk manifest in reduced dimensionality systems. From a practical standpoint, reduced dimensionality systems are becoming important because of rapid miniaturization of electronic circuits. With electronic devices getting smaller by the day engineers have to design smaller transistors. For comparison, the first chip had about 2,200 transistors on it whereas today, hundreds of millions of transistors can fit on a single chip. There are already computer chips that have nanometer sized transistors and future transistors will have to be even smaller. This makes understanding electronics in general and superconductivity in particular in reduced dimensionality samples very relevant.

Let us begin by introducing the specific scales involved and systems of interest. A superconductor with one, two or three dimensions smaller than ξ is in the quasi-two-dimensional (2D), quasi-one-dimensional (1D) or quasi zero dimensional (0D) regime respectively. For most conventional superconductors, ξ is of the order of microns. Therefore, systems falling in the 2D, 1D or 0D category are nanoscale systems. According to Hohenberg-Mermin-Wagner theorem (Hohenberg, 1967; Mermin & Wagner 1966), in these reduced dimensionality systems, fluctuations should destroy superconducting order even at low temperature. In 2D samples, the Berezinski-Kosterlitz-Thousless transition occurs, enabling superconducting order to exist at low temperature. However, the existence, limits

*Corresponding author

and nature of superconductivity in 1D remain a subject of interest. Fortunately, the advent of advanced synthesis techniques like electron beam lithography has enabled scientists to probe the nature of superconductivity in quasi-1D samples. In these systems, superconductivity exhibits many novel phenomena that shed light on the nature of superconductivity. In addition, the aforementioned miniaturization of electronic devices is opening up new horizons for applications of 1D nanowires, and need for understanding superconductivity at this scale. These quasi-1D systems therefore form the basis of the studies described in this chapter.

In this chapter, we hope to provide a comprehensive picture of superconductivity in nanoscale systems starting from synthesis techniques currently in use to examples of the new physics these systems are helping in uncovering. The systems that we focus on are quasi-1D nanowires and nanobelts. In the synthesis section, we will give a brief overview of the common techniques currently in use for making nanoscale samples, especially nanowires. The synthesis and manipulation of these samples can be extremely challenging. Many of the more advanced techniques are continuously evolving and have merited chapters and books on their own. We will include references to some of these more detailed descriptions of the techniques. In the section 3, we will discuss some unexpected discoveries in quasi-1D nanowires and nanobelts. Some of the novel phenomena discussed include macroscopic quantum phenomena, extremely long range proximity effects, the counter-intuitive anti-proximity effect and superconductivity in new materials amongst others. We hope to provide a glimpse of the measurements performed as well as some physical insight into the mechanism behind these phenomena. Finally and most importantly, we will discuss the potential of these new discoveries to be used in technology. The potential for application has not been the least of the reasons why superconductivity continues to capture the imagination of scientists and engineers alike even 100 years after its discovery.

2. Synthesis

The first controlled fabrication of nanowires started in the late 1980s. Early experiments used a top-down approach where a large piece of the material was taken and whittled down using an electron beam to the required size (Knoedler, 1990). Most approaches to nanowire synthesis used today are however bottom-up: where the nanowire is assembled from smaller particles.

2.1 Electrochemical synthesis

Electrochemical synthesis is an inexpensive and versatile method that yields high quality nanowires in a large number. Its limitation is that it is only useful for materials that can be electrochemically deposited from solution (like metals) and its application to semiconductor and non-elemental nanowires is possible but limited. It is a bottom-up approach in which wires are assembled atom by atom from an electrolytic solution with or without an applied potential. Electrochemical synthesis can further roughly be categorized into restrictive template based electrodeposition and active template assisted electrodeposition (Bera, 2004).

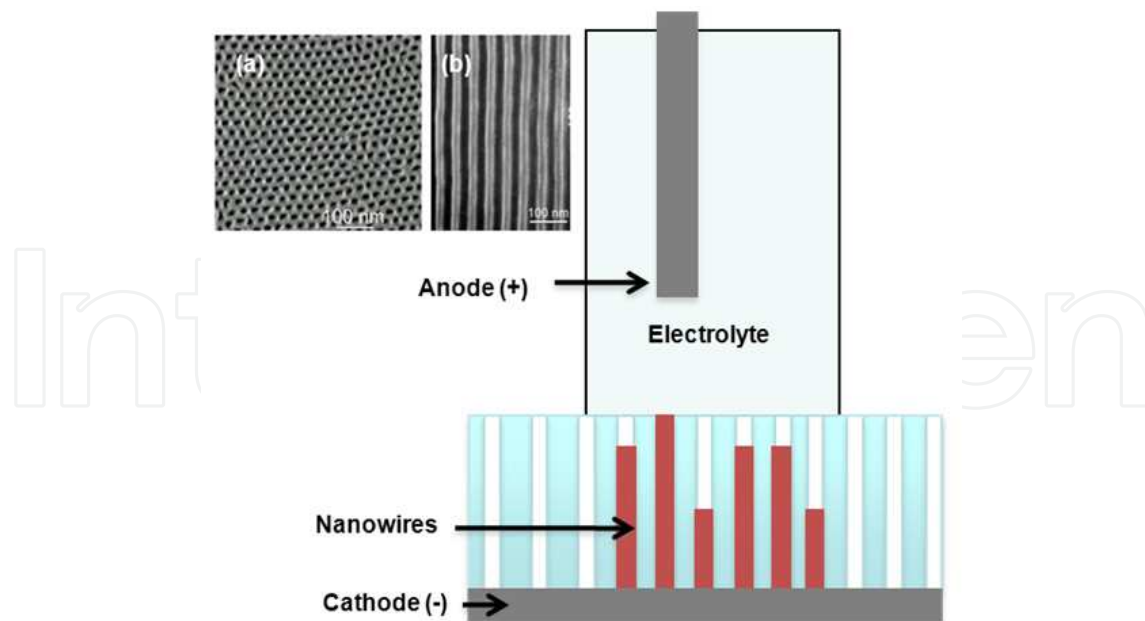


Fig. 1. A schematic of the setup used to electrodeposit nanowires into the pores of a track-etched polycarbonate or anodized oxide (AAO) membrane. The inset shows scanning electron micrographs of (a) a cross section of an AAO membrane and a (b) longitudinal section of an AAO membrane. The regularly arranged pores meant for deposition of nanowires can be seen.

For restrictive template based electrodeposition, commercially available track etched polycarbonate or anodic aluminum oxide (AAO) filtration membranes are used as templates. The pores in these membranes are created by irradiating the membrane with energetic heavy ions and anodizing in acid respectively (Lee, 2006). The resultant pores are parallel to each other and perpendicular to a cross section of the membrane (insets of figure 1). The length and diameter of the nanowire can be controlled by changing the thickness and the pore size of the membrane. The typical pore density varies from 10^8 to 10^{11} pores/cm² which even with low filling fractions yields a large number of nanowires. A schematic of the electrochemical cell typically used is shown in figure 1. For use in electrodeposition, silver or gold is thermally evaporated on one surface of the membrane closing off the pores on that side. This evaporated layer acts as the cathode for electrodeposition. The membrane is then immersed in an electrolyte containing cations of the material(s) to be electrodeposited. A counter electrode and sometimes a reference electrode are put in the circuit and a potential is applied. Since the membranes are insulating, the metal evaporated on one surface acts as the cathode through which the current flows. As the open side of the template is exposed to the electrolyte, positively charged ions move towards the metal at the bottom of the pore. When they reach the metal, they accept electrons and get reduced to their metallic form. When the pores are filled with material, the deposition is halted. The membrane can be dissolved away and the nanowires are released for further use. Variations of this process are used to deposit multilayered nanowires and nanotubes. Some metals like gold can be deposited without an applied potential in an electroless process (Menon & Martin, 1995). In another variation, the pores of the membrane are wet by a precursor followed by thermal decomposition leading to formation of either nanowires or nanotubes in the pore (Nielsch et al., 2005).

The formation of nanostructures in the active template-based synthesis results from preferential electrodeposition of atoms or molecules at hole and defect sites on the electrode surface. Once the initial layer of atoms is crystallized on the defect site, subsequent atoms also preferentially deposit at the site leading to formation of different nanostructures. The preparation of the electrode surface plays a major role in determining the morphology and structure of the electrodeposited nanostructure. Other nanosynthesis techniques like photolithography have been used in conjunction with this technique. Photolithography is used to create nanostructures on the electrode surface into which the required material is then electrodeposited (Yang et al., 2008).

2.2 Lithography

Lithography translates to 'stone writing' and originally referred to the art of writing text on stone. Modern lithographic techniques find a wide variety of uses in the printing process. Our foci of interest for this section are, however, micro-lithographic processes like photolithography and electron beam lithography (EBL) with which most top down nanofabrication processes start. Photo-lithography is the more popular of the two processes and is used for manufacturing of semiconductor microchips. EBL, although more expensive, offers significantly improved resolution, sometimes going down to a few nanometers. Figure 2 shows a schematic of the lithography process.

The substrate (most often doped silicon coated with an insulating layer of silicon oxide or silicon nitride) is spin coated with a photo resist or e-beam resist. The choice of resist depends on the resolution required, spacing of features and thickness of metal to be evaporated post lithography. The resist is baked for hardening. In case of photo-lithography a hard mask is used with the required pattern made on it. In case of EBL, a 'soft' mask drawn using computer software like L-Edit is used. The areas within the pattern are exposed to either UV light for photolithography or an electron beam for EBL. The exposure time and beam-current used depend on the resolution required and the feature size. The exposure of the resist causes it to undergo a chemical reaction. The substrate is then soaked in a developer. In case of positive resist (as depicted in figure 2), the parts of the resist exposed to the beam and chemically altered are dissolved by the developer. For negative resist, the parts not exposed to the beam are dissolved away. The substrate is now left with resist everywhere except for places where the pattern should be. The required material is now evaporated on the substrate. This material fills the blanks left by the dissolved resist and also covers up the remaining resist. The substrate is then taken for the 'lift-off' process where it is dipped in a solvent that dissolves away the remaining resist. The material covering the resist is stripped away with the resist, and only the material in the pattern remains on the substrate. Lithography has the advantage of being an extremely flexible technique that can be used to create a large variety of shapes and sizes of nanostructures. It is also a technique most likely to become scalable to uses in chip design and manufacture in the future. The disadvantage is that lithography, especially EBL tends to be very expensive and the resulting nanostructures are most often granular (this depends on the evaporation conditions). A more in-depth description of lithography can be found in (Madou, 2002).

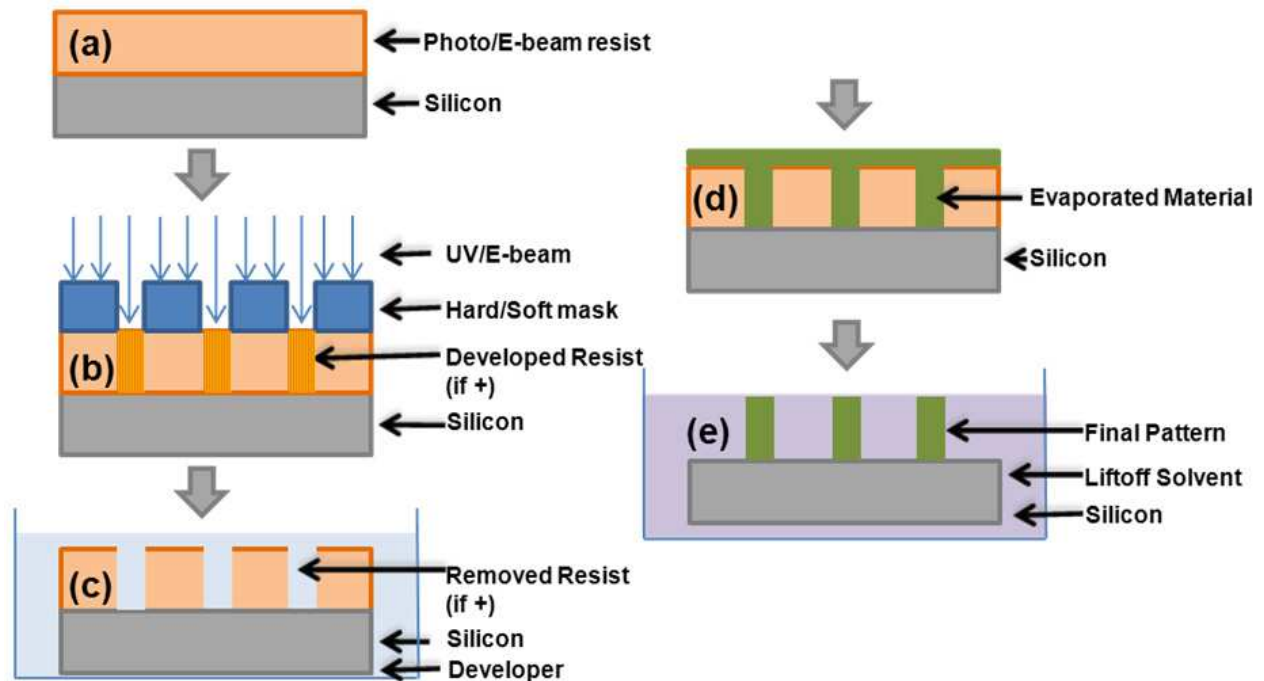


Fig. 2. A schematic of the lithography process for making nanostructures (a) a layer of resist is spin-coated on the substrate, (b) the resist is exposed to either UV radiation in case of photolithography or an electron beam in case of electron-beam lithography through a mask which has the required pattern cut out from it, (c) the substrate with the resist is soaked in a developer which removes the parts of the resist that were exposed to radiation earlier (in case of positive resist) or parts that were not exposed to radiation earlier (in case of negative resist), (d) material is evaporated onto the substrate with the resist acting as a mask, (e) the substrate is soaked in a solvent that dissolves the remaining resist and also the layer of evaporated material on the resist. This 'lift-off' process only leaves behind the material evaporated directly on the substrate in step (d).

2.3 Chemical vapor deposition

The technique of Chemical Vapor Deposition (CVD) is mostly used for the synthesis of thin films. The process is very versatile and allows for growth of amorphous, epitaxial, monocrystalline and polycrystalline films. The CVD equipment consists of a tube-like, chamber in which the substrate for synthesis is placed, a mechanism to heat the substrate, a gas handling system which is used to introduce vapors into the chamber and an exhaust from which the waste vapors escape.

For the synthesis, a precursor dissolved in a solvent or in the form of an emulsion is vaporized and introduced into the chamber where some of the precursor mixture deposits on the substrate. The substrate is then heated causing the precursor mixture to decompose and the solvent to evaporate away. A layer of the required precursor is thus left on the substrate. If a metal organic compound is used as the precursor, the method is referred to as Metal-Organic Chemical Vapor Deposition (MOCVD). A slight variation of this

technique is also used for nanowire and nanotube growth under the name of Vapour Liquid Solid method (VLS). This method was developed in 1964 for the growth of Silicon whiskers (Wagner & Ellis, 1964). In the first step, a layer of a solid impurity such as gold is thermally evaporated on the substrate. The substrate is then heated so that liquid droplets of an alloy of the impurity and the substrate form on the surface. In the next step, like the CVD method, a vaporized solution of the desired material is introduced into the chamber. The liquid droplets formed on the substrate in the earlier step act as catalysts in the reaction to deposit atoms of the required material on the substrate. By a continuation of this process, a nanowire on the substrate is formed. A schematic of this process is shown in figure 3. This technique has recently been used for successful synthesis of topological insulator nanoribbons (Peng et al., 2010). Using lithography in conjunction with this technique also allows for ordering the nanowire growth. Recently a variation of the CVD method has been used to grow very large aspect ratio (length:diameter) nanowires in microstructured optical fibers (Sazio et al., 2006). The advantage of this method is its adaptability to a wide range of materials. The disadvantages mostly involve safety and contamination as poisonous and pyrophoric (ignite in contact with air) precursors are used.

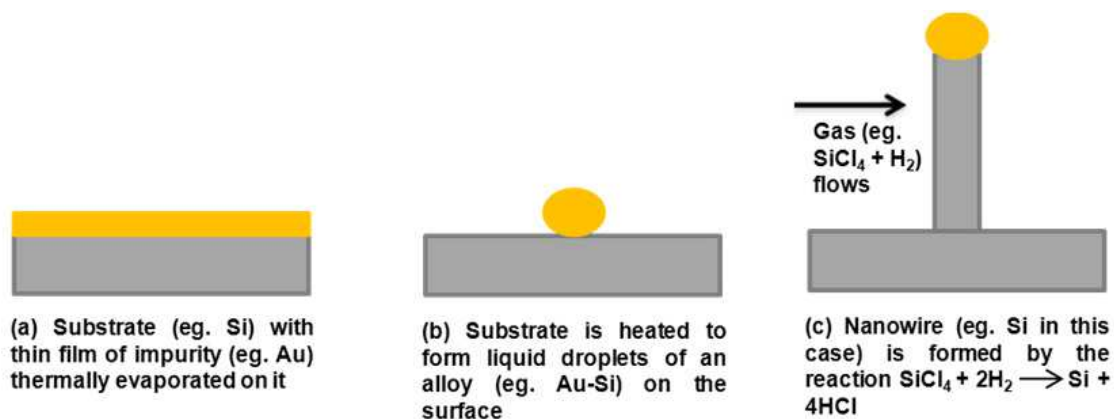


Fig. 3. A schematic of the chemical vapor deposition process modified to the vapor-liquid-solid method for nanowire growth.

2.4 Molecular beam epitaxy

Molecular Beam Epitaxy (MBE) is a refined form of thermal evaporation. In MBE, directed neutral beams of atoms or molecules of a substance being evaporated get deposited on a substrate. The major difference from thermal evaporation is that the deposition is extremely slow, allowing for atomic layer by atomic layer epitaxial growth. The samples grown by MBE are high quality single crystals. The very slow growth rate requires the evaporation to be done in ultra-high vacuum to keep the contamination levels in check. The apparatus to fulfill these requirements is considerably complicated (schematics of a typical MBE chamber are shown in figure 4). In addition, the substrates for sample growth also have to be of very high quality. This technique generates extremely smooth and thin samples with a high degree of compositional control and crystal perfection. The payoff is its high cost. The method is largely used in the synthesis of thin films but, can also have applications to nanowire growth (section 3.6). Further details of this method of sample synthesis can be found in (Arthur, 2002).

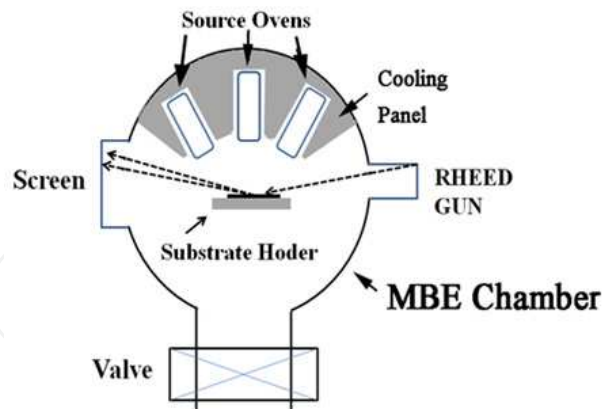


Fig. 4. A molecular beam epitaxy chamber.

In addition to these commonly used techniques, several other ingenious methods have been used for nanostructure synthesis. These include DNA (Stoltenberg & Woolley, 2004) and carbon nanotube template nanowire synthesis (Bezryadin et al., 2000) and microbial nanowires (Reguera et al., 2005) amongst others.

3. Novel phenomena – What they imply and their potential applications

When a material transits from a normal to a superconducting state, electrons with opposite spins pair up. As mentioned in the introduction, this pair is called a 'Cooper pair'. Once part of a Cooper pair, the two electrons can be described by a single quantum mechanical wave function $\psi = |\psi|e^{i\phi}$. The spatial extent of this wavefunction, or the 'size' of a cooper pair, is known as the coherence length (ξ) and ϕ is the phase of the wavefunction. If the superconducting state is made possible by electrons 'holding hands' to form Cooper pairs, what happens to the superconductivity when the diameter of the nanowire the Cooper pairs are supposed to go through is smaller than ξ ? Do the Cooper pairs break up and is superconductivity destroyed in these quasi-1D systems? This dilemma lies at the root of why superconductivity in quasi-1D systems is different. It is also responsible for the plethora of novel phenomena seen on studying superconductivity in quasi-1D wires as described below.

3.1 Phase slips – Thermally activated and quantum

In the superconducting state, the phase ϕ is spatially coherent. This means that if the phase at any one point is known, the phase at any other point can be predicted. Fluctuations (thermal and quantum) lead to loss of phase coherence in superconducting samples from time to time. The region where the coherence is lost becomes temporarily normal (ϕ becomes ill defined). The spatial extent of such a region is given by ξ . For 3D or 2D samples, these normal regions without phase coherence do not affect the transport measurement as the charge carriers can bypass them. In a quasi-1D sample however, since the diameter (d) $<$ ξ , the normal region encompasses the entire cross section of the wire and cannot be bypassed. Therefore, phase slips result in a loss of superconductivity in quasi-1D systems. Mathematically, this can be understood using Josephson relation:

$$V = \frac{d(\Delta\phi)}{dt} \quad (1)$$

Here, V is the voltage across the system, t is the time, ϕ is the phase, and $\Delta\phi$ is the phase difference across the system. In a phase slip event, the phase at some point in the sample becomes ill defined. When it recovers, the value of $\Delta\phi$ is changed by 2π causing a finite voltage V to appear across the system and hence, a loss in superconductivity. So, in a phase slip event, the system essentially goes from a superconducting state with some value of $\Delta\phi$ to a superconducting state with a value of $\Delta\phi$ different from the previous value by 2π . To go from one state to another, the system needs to cross a potential barrier (figure 6). The energy to cross the barrier can be provided by thermal energy (thermally activated phase slips) or by quantum fluctuations (quantum phase slips). Extensive experiments attempting to see both kinds of phase slips have been done.

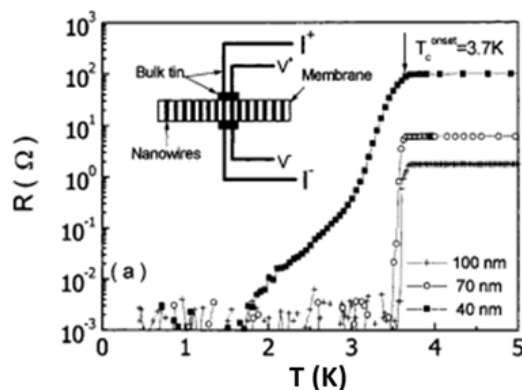


Fig. 5. (Tian et al., 2003) Resistance vs. Temperature measurements on tin nanowire arrays embedded in track-etched polycarbonate membranes and squeezed between bulk tin electrodes. The schematics of the measurements are shown in the inset. The measurements shown here are performed on three different arrays which the wires are 40 nm, 70 nm and 100 nm in diameter. For the 40 nm diameter tin nanowires rounding of the superconducting transitions and a long resistance tail can be seen.

Transport measurements of resistance (R) as a function of temperature (T) of quasi-1D samples differ from bulk samples in two ways. The first is a rounding of the superconducting transition and the second is the presence of a superconducting tail in the quasi-1D samples. These two features can be seen to appear in figure 5. The figure shows R vs. T measurements performed on single crystalline tin nanowire (SnNW) arrays embedded in polycarbonate membranes contacted with bulk tin electrodes (Tian et al., 2003). A schematic of the measurement is shown in the inset of figure 5. Measurements are performed on 3 different sets of nanowires of diameters 100 nm, 70 nm and 40 nm. The transition for the 100 nm and 70 nm diameter nanowires is sharp and the resistance falls from the normal state value to zero in a temperature interval of 90 mK. The transition for the 40 nm nanowire on the other hand, is rounded and also has a long resistive tail stretching from 1.8 K to 3.7 K, a range of 1.9 K. These two features are attributed to thermally activated (TAPS) and quantum phase slips (QPS) respectively.

In TAPS, the system crosses the energy barrier between the superconducting states whose values of $\Delta\phi$ differ by 2π with the help of thermodynamic fluctuations (figure 6). The resistance due to TAPS below the critical temperature of the superconducting transition (T_c) can be written as (Langer & Ambegaokar, 1967; McCumber & Halperin, 1970):

$$R_{TAPS} \propto e^{-\Delta F/k_B T} \quad (2)$$

where ΔF is the free energy barrier between the two states and the proportionality constant is related to the attempt frequency and the temperature. For low excitation currents $\Delta F = \sqrt{2}\sigma H_c^2 \xi / 3\pi$ where σ is the cross sectional area, H_c is the critical field and ξ is the coherence length. As the temperature decreases, the size of the free energy barrier relative to $k_B T$ increases, leading to a rapid reduction in the thermal-activation rate. At very low temperature this rate becomes negligible. TAPS is therefore, only important close to T_c and is associated with the rounding of the superconducting transition seen in the SnNW. However, it cannot explain the resistive tail that persists to low temperatures. To explain the resistive tail, some other process by which the phase can relax has to be taken into account. QPS, or the tunneling through the energy barrier (figure 6) is the dominant process at low temperatures (Giordano, 1988, 1991; Giordano & Schuler 1990). A heuristic argument (Giordano, 1994) suggests that the resistance given by the QPS will follow the same form as R_{TAPS} except for the energy scale being given by $\hbar\omega = \hbar/\tau_{GL}$ instead of $k_B T$. Here, τ_{GL} is the Ginzburg Landau relaxation time given by $\tau_{GL} = \pi\hbar/8k_B(T_c - T)$. Therefore,

$$R_{QPS} \propto e^{-\alpha\Delta F\tau_{GL}/\hbar} \quad (3)$$

where α is possible numerical factor. QPS has fascinated experimentalists and theorists alike for almost 2 decades now because of its tremendous implications (Altomare et al., 2006; Lau et al., 2001). The observed resistance tail is an example of macroscopic quantum tunneling because a macroscopic, measurable quantity (resistance) is changing in response to a quantum tunneling event. It has been suggested that QPS in nanowires can be used to realize a superconducting quantum bit that can have much lower $1/f$ noise than existing quantum bits using Josephson junctions (Mooij & Harmans, 2005). These quantum bits not using Josephson junctions can form a new basis for superconducting quantum computing.

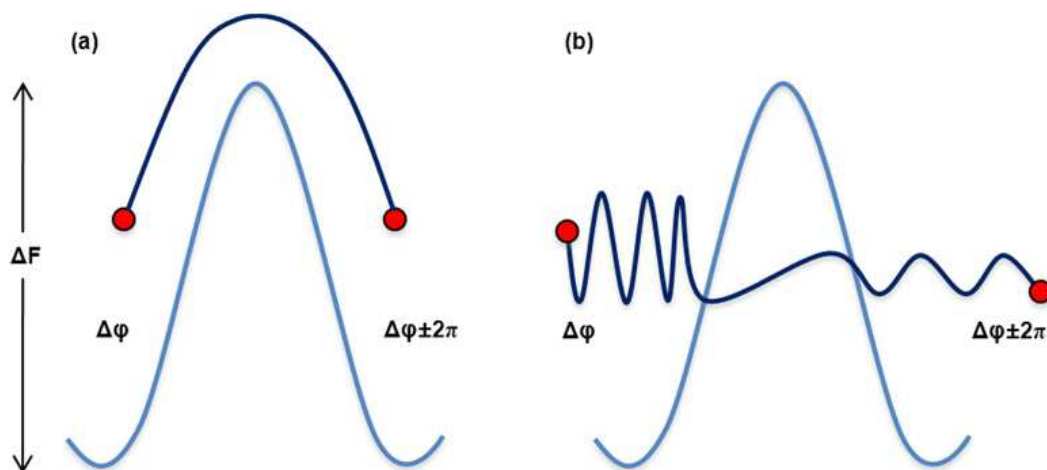


Fig. 6. A representation of the (a) the thermally activated phase slip where thermal energy allows the system to go over the energy barrier separating two superconducting states, (b) quantum phase slips that allow the system to tunnel from one superconducting state to the other even at low temperatures. The two superconducting states in question have the phase difference between the two ends of the superconductor ($\Delta\phi$) different by 2π .

3.2 Long range proximity effect in ferromagnetic nanowires

In a singlet (s-wave) superconductor, the spins of the electrons making a Cooper pair are antiparallel (the spin part of the wavefunction is given by $|\uparrow\downarrow\rangle - |\downarrow\uparrow\rangle$). The spins of electrons in a ferromagnet, on the other hand, are aligned parallel to each other. This incompatible spin order between singlet superconductors and ferromagnets makes for new and interesting physics when the two are placed in contact with each other. When a superconductor is placed in contact with a normal metal, the Cooper pairs in the superconductor tunnel into the normal metal, making it partially superconducting. This is known as the superconducting proximity effect. The distance to which Cooper pairs survive in the non-superconducting material is the range of the proximity effect. This range, for a bulk normal metal can be $\sim 1\mu\text{m}$. For a bulk ferromagnet however, the incompatible spin order ensures that the singlet Cooper pair cannot survive beyond a few nanometers. This expectation has been confirmed in macroscopic (Fe, Ni)-In junctions (Chiang et al., 2007) and submicrometre Ni-Al structures (Aumentado & Chandrasekhar, 2001) where the spatial range of the proximity effect is limited to $\sim 1\text{ nm}$. In mesoscopic ferromagnet-superconductor hybrid structures, a surprisingly long range proximity effect has been found (Bergeret et al., 2005; Giroud et al., 1998; Keizer et al., 2006; Pena, V. et al., 2004; Petrashov et al., 1999; Sosnin et al., 2006). In particular, a recent experiment detected super-current in half-metallic ferromagnet CrO_2 thin film sandwiched between two singlet superconducting electrodes separated by $1\mu\text{m}$ (Keizer et al., 2006). To account for the long range proximity in these systems, the superconductivity was attributed to the spin triplet (spin wavefunction given by one of $|\uparrow\uparrow\rangle$, $|\downarrow\downarrow\rangle$ or $|\uparrow\downarrow\rangle + |\downarrow\uparrow\rangle$ which do not preclude parallel spins) rather than the spin singlet state. The formation of the spin triplet state requires the presence of a region of non-collinear magnetization. This region, in the case of an experiment on a Co thin film was provided by a thin weakly superconducting CuNi or PdNi layer between the superconducting Nb and the ferromagnetic Co film (Khaire et al., 2010).

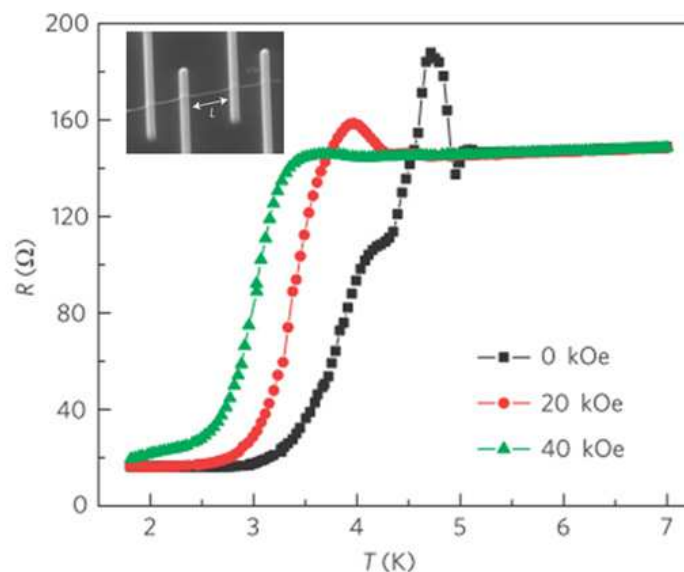


Fig. 7. (Wang et al., 2010a) Resistance vs. Temperature measurements for a 40 nm diameter, 1.5 μm long cobalt nanowire at different applied fields. The applied fields are perpendicular to the wire. The inset shows an scanning electron micrograph of the cobalt wire contacted with 4 focused ion beam deposited superconducting tungsten electrodes.

The occurrence of this long-range proximity effect was also reported in ordinary, hard ferromagnetic crystalline nanowires in standard 4-probe measurements (Wang et al., 2010a). The Co and Ni nanowires (CoNW and NiNW) were synthesized using template based electrodeposition into the pores of a track-etched polycarbonate membrane. The CoNW were single crystalline while the NiNW were polycrystalline. The nanowires were released from the membrane and dispersed on a Si/SiN substrate and contacted by a focused ion beam (FIB) system with superconducting tungsten (W) electrodes. The R vs. T measurements at different applied fields (H) on a 40 nm diameter, 1.5 μm long CoNW are shown in figure 7 (the inset shows the measurement geometry). A large resistance drop (to 11% of the normal state value) at the T_c of the W electrode suggests a very long range (~ 500 nm) proximity effect in the CoNW. The range of the proximity effect is smaller (~ 375 nm) in thicker (80 nm) diameter nanowires. The expected singlet coherence length in Co nanowires is given by $\xi_F = \sqrt{\hbar D / k_B T_{Curie}}$ (Keizer et al., 2006), where T_{Curie} is the Curie temperature and $D = (1/3)v_F l$ is the electron diffusion constant (here, v_F is the Co Fermi velocity $\sim 10^8$ cm s^{-1} and l is the mean free path). The experimentally measured resistivities yield a singlet coherence length of 3.3 nm for the sample shown in figure 7, which is much smaller than the observed coherence length of 500 nm. The superconductivity in this system also may be triplet in nature. It has been suggested that the region between the W electrodes and the CoNW is damaged by the FIB process and may thus be largely inhomogeneous and act as a seeding ground for triplet pairing. Another explanation may be that the surface of the CoNW and NiNW is not ferromagnetic and the superconducting proximity effect is only on the non-ferromagnetic surface of the nanowires. In (Konschelle et al., 2010) it is suggested that a phase sensitive measurement, experimentally testing the Josephson current-phase relationship can be used to discriminate between the two scenarios.

Other than the extremely long-range proximity effect, another striking feature visible in figure 7 is the very large resistance peak (25% of the normal-state resistance) found between 5 K and 4.5 K, just above the temperature of the superconducting resistance drop. This 'critical peak' is preceded by a small dip on the high-temperature side of the peak. Measurements in both warming up and cooling down scans show an absence of hysteretic behavior. Both the peak and the superconducting drop are stable on cycling the sample to room temperature. This peak does not conform to charge imbalance peaks typically seen in superconducting mesoscopic systems since a very large magnetic field is required to destroy it. Charge imbalance peaks on the other hand are destroyed by very small applied fields (Santhanam et al., 1991). Another mechanism used to explain resistance peaks in Fe-In junctions is spin accumulation (Chiang et al., 2007). In that case, however, the absolute peak value (ΔR) was many orders of magnitude smaller ($10^{-8}\Omega$), as was the relative change from the normal-state resistance ($\Delta R/R \sim 0.05\%$). Furthermore, spin accumulation would assume that the induced superconductivity is singlet in nature, which seems inconsistent with the long range proximity effect. A satisfactory explanation of this peak is yet to be found.

The long range proximity effect in ferromagnets offers the possibility of combination of the zero-resistance supercurrents of superconductors with the spin alignment of ferromagnets. This has tremendous implications for spintronics (Eschrig, 2011). Superconducting spintronic devices offer elements of non-locality (if the superconducting coherence length is larger than the nanoscale device), coherence (electrons in a cooper pair are coherently

coupled even if they go in separate electrodes) and entanglement (stemming from coherence), all of which are essential for quantum computing. The availability of triplet supercurrents may also revolutionize the field of spintronics with new spin valves, pumps, switches, transistors and filters.

3.3 Anti-proximity effect

When a superconductor is placed in contact with a normal metal, signs of superconductivity appear in the normal metal. This 'proximity effect' is a much documented and well-studied phenomenon. However, a number of recent experiments have reported an unexpected 'anti-proximity effect' (APE) in zinc nanowires (ZnNW) contacted with bulk superconducting electrodes (Chen et al., 2009, 2011; Singh et al., 2011; Tian et al., 2005, 2006). In the original experiment, (Tian et al., 2005) ZnNW 6 μm in length embedded in track-etched polycarbonate membranes were squeezed between superconducting bulk electrodes for two-electrode transport measurements (the schematics of the measurement are similar to those shown in the inset of figure 5). In this configuration, the resistance of the long nanowires dominates the overall series resistance, and the contact resistance is minimized as in a 4-electrode measurement. In 70 nm diameter nanowires contacted with bulk tin (Sn) electrodes, the superconducting transitions of Sn at 3.7 K and of the ZnNW at 1 K were both seen, consistent with expectation. However in 40 nm diameter nanowires, the transition for Sn was seen but the superconducting transition for Zn was absent. When the Sn electrodes were driven normal by a magnetic field of 300 Oe, the superconducting transition of Zn reappeared. The APE in the 40 nm Zn wires was replicated with indium (In) and lead (Pb) electrodes (Tian et al., 2006a). The experiment with In electrodes showed that the APE in the 40 nm Zn wires was switched off precisely when the magnetic field was increased above the critical field of In (Tian et al., 2005). With Pb electrodes, the strength of APE was weaker and there was no obvious suppression of superconductivity in the ZnNWs in resistance measurements as a function of temperature or magnetic field. The APE however, could be detected in the critical current (I_c) of the Zn wires. Specifically the I_c of a Pb/Zn/Pb sample showed a dramatic increase when the magnetic field was increased towards the critical field (H_c^{Pb}) of Pb. Only at fields higher than H_c^{Pb} did the I_c of the ZnNWs show the 'normal' behavior, namely a decrease with increasing field (figure 8). Similar I_c behavior vs. magnetic field was also confirmed in aluminum nanowire (AlNW) arrays embedded in anodic aluminum oxide membrane contacted with In electrodes (Singh et al., 2011) and in four electrode measurements on e-beam assisted evaporated granular ZnNWs (Chen et al., 2009, 2011). The nanowires and the electrodes for this experiment were evaporated in a single step using an e-beam lithographically fabricated mask. The authors attributed the increase in I_c to the creation of quasi-particles as the bulk electrodes are driven toward the normal state by the external magnetic field. In all these experiments, a magnetic field was used to see the APE. It is therefore natural to question whether the APE is caused by the magnetic field. To answer this question an experiment was performed where two single crystalline AlNW grown using electrodeposition (Singh et al., 2009) of the same diameter (70 nm) and length (2.5 μm) were contacted with superconducting W and normal platinum (Pt) electrodes using the FIB process. The I_c of the wire contacted with the superconducting electrode was found to be significantly smaller than the I_c of the wire contacted with the normal electrode (figure 9) indicating suppression of superconductivity of the AlNW because of the bulk superconducting electrode. As there were no applied magnetic fields in this experiment, this

served to definitively decouple the APE seen in the 70 nm wire from negative magnetoresistance caused by a weak applied magnetic field seen in other experiments (Herzog et al., 1998; Rogachev et al., 2006; Xiong et al., 1997). The phenomenon also shows a strong dependence on the diameter and length of the sample and the nature of the measuring electrodes. It is not seen in 200 nm AlNW and is very weak in 50 μm long AlNW. It is also weaker in ZnNW with Pb electrodes compared to ZnNW with In electrodes.

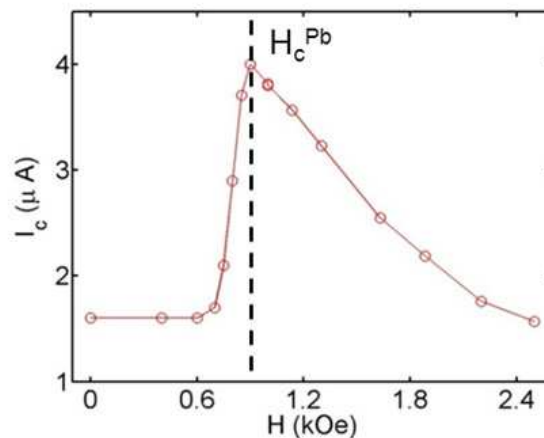


Fig. 8. (Tian et al., 2005) An enhancement in the critical current (I_c) of a zinc nanowire array squeezed between superconducting lead electrodes is seen when the magnetic field is increased toward the critical field of the bulk superconducting lead electrodes contacting the nanowires. The critical current peaks at the critical field H_c^{Pb} of the electrodes.

A theoretical model applicable to this system was given by Fu et al. (Fu et al., 2006) generalizing the resistively shunted Josephson junction to include superconducting nanowires. In this model the nanowire array connected to the two bulk superconducting electrodes is modeled as a nanowire in series with two resistors and in parallel with a capacitor. When the electrodes are normal, the resistors in series provide a medium for dissipation of quantum phase slips, thus stabilizing the superconductivity. When the electrodes are superconducting, this dissipation path disappears and the wire becomes normal. A similar explanation was proposed to understand the results of the experiments on granular Zn nanowires. Although the model agrees with the results qualitatively, it does not explain how the strength of the effect depends on the contacting electrode in AlNWs or ZnNWs. In addition to the material of the electrodes, other important parameters in these experiments are the 'characteristic' diameter and the length of the nanowires that define the presence or absence of APE. It is difficult to obtain quantitative predictions for these quantities from this model. A more quantitative mechanism using the time independent Ginzburg-Landau equations was proposed by Vodolazov (Vodolazov, 2007). The qualitative behavior of the system is reproduced at temperatures close to T_c and the authors expect traces of this behavior to exist at low temperatures also. The mechanism of Vodolazov uses the fact that the diameters of the wires are smaller than the superconducting coherence length to model them as a 1D system. The coherence length for the AlNWs in these experiments can be estimated using the value of $\xi_0 l$ (where l is the mean free path) as $4 \times 10^{-16} \Omega \text{ m}^2$, the dirty limit coherence length $\xi(0) = 0.855(\xi_0 l)^{0.5}$ and 1600 nm as the value for ξ_0 . $\xi(0)$ is estimated to be ~ 50 nm. In comparison, APE was seen 70 and 80 nm diameter AlNW but, not in 200 nm diameter nanowires. In ZnNWs, the $\xi(0)$ was estimated to be ~ 150 nm and the APE was seen in 40 nm diameter nanowires but

not in 70 nm diameter nanowires (Tian et al., 2005). The model also predicts a weakening or absence of the APE in nanowires with length $L > \Lambda_Q$ (the charge imbalance length). The charge imbalance length of the Zn NWs was calculated to be 22 μm (Vodolazov, 2007) and that of AlNW to be 19 μm (Singh et al., 2011), and this was used to explain the relatively weak APE in long $\sim 35 \mu\text{m}$ Zn and $\sim 50 \mu\text{m}$ AlNWs. Lastly, this mechanism uses an external magnetic field to model the critical current enhancement seen in the APE and the APE has now been seen in the absence of an external magnetic field.

The APE is a counterintuitive phenomenon that challenges our understanding of superconductivity. The phenomenon is qualitatively consistent with the Vodolazov model, but the presence of the phenomenon without an applied field shows that further theoretical work is needed to gain a more complete and quantitative understanding of the APE. A complete picture of the mechanism behind this behavior will offer great insight into superconductivity in nanoscale systems and perhaps open doors to new applications.

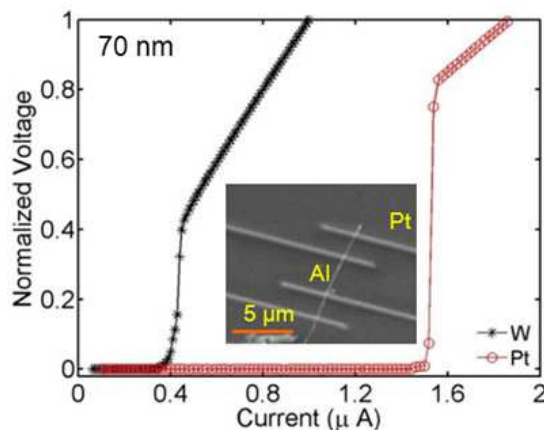


Fig. 9. (Singh et al. 2011) Normalized voltage vs. applied current for two 70 nm diameter, 2.5 μm long single aluminum nanowires at a temperature of 0.1 K. One of the nanowires is measured using normal focused ion beam deposited normal Pt electrodes and the other is measured using superconducting W electrodes. The inset shows a scanning electron micrograph of the aluminum nanowire contacted with the normal platinum electrodes. The nanowire contacted tungsten also looks the same under a scanning electron microscope.

3.4 Mini-gap state

In superconducting nanowires contacted with superconducting electrodes, the counterintuitive APE is seen. What happens when a normal nanowire is contacted with superconducting electrodes? In this situation, in addition to the expected and well-studied phenomenon of the proximity effect, some surprising new phenomena are uncovered. In a recent experiment (Wang et al., 2009a), crystalline gold nanowires (AuNW) 70 nm in diameter were contacted with superconducting W electrodes using FIB. As expected, the superconducting proximity effect caused the short wires (1 μm and 1.2 μm long) to go completely superconducting whereas the longer nanowires (1.9 μm) retained some residual resistivity to the lowest measured temperatures. This gives the range of the proximity effect to be $\sim 600 \text{ nm}$. A surprising feature however, was that the superconducting transition of

the 1.2 μm long wire occurred in two steps at two distinct T_c s (figure 10). In the R vs. H measurements two distinct H_c s were also seen. The two-step drop in resistance is suggestive of two distinct transitions. The higher T_c and H_c are almost same as the corresponding values for the W electrodes. The results are interpreted with proximity induced superconductivity in the nanowire with a small superconducting “mini-gap” δ near the centre of the wire which is different from the gap elsewhere in the wire. The gap near the electrodes in the wire corresponds to the bulk W gap (Δ). This “mini-gap” state is a novel superconducting state not seen in bulk samples.

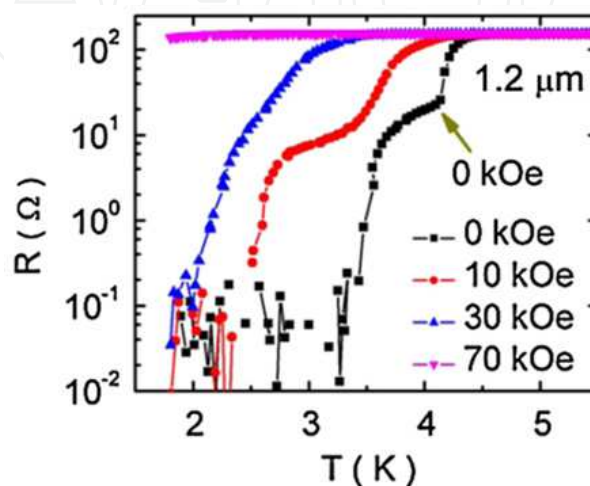


Fig. 10. (Wang et al., 2009a) Resistance vs temperature plots for a 70 nm diameter, 1.2 μm long single crystalline gold nanowire at different magnetic fields applied perpendicular to wire axis. The gold nanowire is contacted with superconducting tungsten electrodes using a focused ion beam system and the measurement shown has been done in the standard four-probe configuration. The superconducting transition can be seen to occur in two steps at two distinct ‘critical’ temperatures.

The R vs. H measurement of a 1.0 μm long nanowire and 1.2 μm nanowire are shown in figure 11 (a) and 11(b) respectively. A small resistance valley is more apparent in the 1.2 μm long nanowire. This resistance valley is associated with the mini-gap state. The details of the temperature evolution of the mini-gap in the R vs. H measurements can be seen in the magnified graph in figure 11 (c). The H_c of the mini-gap is ~ 3000 Oe in comparison to the larger transition H_c corresponding to the W electrode H_c of ~ 80000 Oe (figure 11(b)). The curves have been offset for clarity. At 2.4 K, there is no sign of the mini-gap. At 2.5 K, the resistance suddenly jumps and then quickly drops back to zero at 2.5 kOe. At 2.6 K, this magnetic-field-symmetric resistance fluctuation becomes more clearly developed and the baseline of the fluctuating resistance at fields above the mini-gap region is seen to be smoothly increasing with field. With increasing temperature the mini-gap valley continues to shrink in width, disappearing at $T = 4$ K. Evidence for the mini-gap in proximity structures was also revealed in recent scanning tunnelling microscopy studies (Gupta et al., 2004; Le Sueur et al., 2008; Vinet et al., 2001) and another transport measurement (Lucignano et al., 2010). In addition to the mini-gap state, resistance plateaus can be seen in the R vs. H measurements in the transition region (figure 11(a) and 11(b)).

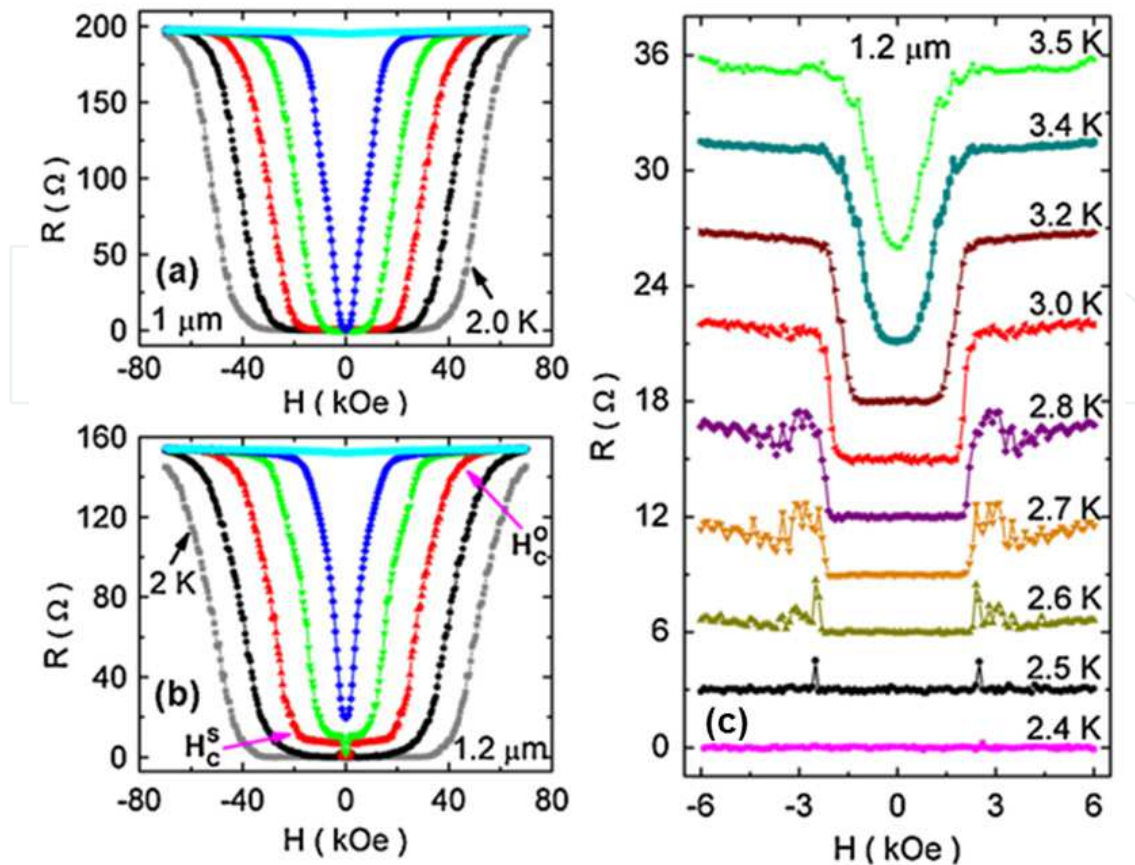


Fig. 11. (Wang et al., 2009a) (a) Magnetoresistance of the 1 μm gold nanowire, from bottom to top, at 2.0 K (gray), 2.5 K (black), 3.0 (red), 3.5 K (green), 4.0 K (blue), and 5.5 K (cyan). (c) Close-up view of (b) near zero magnetic field at different temperatures for the 1.2 μm long nanowire. The curves are offset for clarity; except for 3.5K, the resistance in all plots is zero at zero field. The mini-gap state seen as the small resistance valley is apparent in the 1.2 μm long nanowire but, not in the 1 μm long nanowire.

In figure 12, plots of the numerical derivative dR/dH of the 1 μm and 1.2 μm nanowires are shown as a function of H at 3K (He & Wang, 2011). The applied field is perpendicular to the wire. This differential magnetoresistance shows uniform oscillations with increasing field with a period of $\phi_0/(2\pi r^2)$ (where, $\phi_0 = h/2e$ is the superconducting flux quantum, $r = 35 \text{ nm}$ is the radius of the nanowire). The period of the differential resistance plateaus can be explained by theorizing that each step in resistance is caused by a phase slip. The phase slips are created by vortices moving across the wire that are generated by the perpendicular magnetic field. The extraordinary feature in this experiment is that the nature of the gap in the proximity induced superconductivity in the AuNW allows for generation of individual vortices one at a time along the nanowire. The gap in the middle of the wire is the smallest and is the first site for single vortex creation. As the field is increased the vortex moves to higher gap regions and a new vortex is created in the center of the wire. As a result, the resistance of the Au wire increases with increasing field step by step so that the generated vortices move continuously across the wire. This is very different from the well-known behavior of superconductors where when the field is increased beyond a critical value, vortices proliferate all at once and the superconductivity is destroyed. In figure 12, the numbers assigned to each peak are theorized to be associated with the number of vortices in

the nanowire. An interesting fact is that if the spatial extent of each vortex is taken to be limited by the diameter of the nanowire, the total number of vortices that will fit in the 1 μm nanowire is $1\mu\text{m}/70\text{nm} = 15$ which in fact corresponds to the number of peaks seen before the wire becomes normal.

The implications of the range of new phenomena discovered in proximity induced superconducting nanowires are profound. First of all, the fact that AuNW up to 1.2 μm long act as a superconductor provides us a large number of 'new' superconductors that can be used in nanoscale circuitry. The 'mini-gap' state is a new superconducting state that opens new avenues for exploration of the physics of nanoscale superconductors. The ability to introduce and manoeuvre vortices one by one in the proximity induced superconducting system is a first. If scalable synthesis for such samples can be developed, the manoeuvrable vortices can be utilized as memory units in quantum computing.

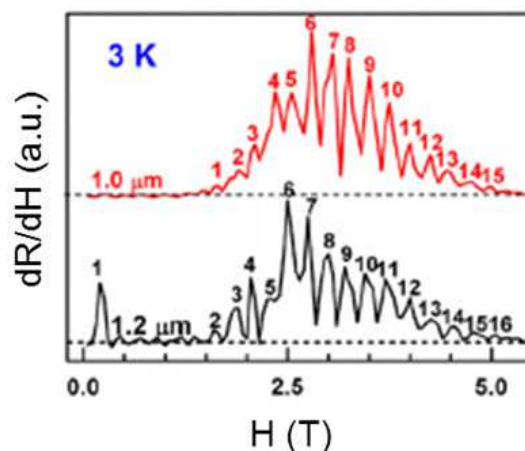


Fig. 12. (He & Wang, 2011) The differential magnetoresistance as a function of magnetic field of the 1.0 and 1.2 μm long gold nanowires measured at $T = 3\text{K}$. The dashed lines represent $dR/d|H| = 0$ for the two wires. There are small oscillations of the value of $dR/d|H|$ around zero H , possibly due to the limited resolution in the R and H readings in low magnetic field. The clearly resolved peak at about 1.65 T was picked as the first peak of the 1.0 μm wire. The peak at the differential magnetoresistance shows uniform oscillations with B of 0.25 T. The number on the peak was theorized to match with the number of vortices in the nanowire.

3.5 New superconducting materials – Bismuth

Bi has an extremely small Fermi surface (FS) (just 10^{-5} of the Brillouin zone), low carrier density ($\sim 3 \times 10^{17} / \text{cm}^3$ at 2 K), small effective carrier mass ($m_e^* < 0.003$ free electron mass for electrons along the trigonal direction) (Liu & Allen, 1995) and very long electron mean free path (exceeding 2 μm at room temperature) (Hartman, 1969). These properties distinguish Bi from other metals and make it particularly suitable for studying quantum phenomena. A most striking example of superconductivity behaving differently in nanoscale systems was observed in granular bismuth nanowires (BiNW) electrodeposited in track-etched polycarbonate membranes (Tian et al., 2006b). Bulk rhombohedral Bi is a semimetal with no superconducting transition observed down to 50 mK under ambient pressure. In granular BiNW however, 70 nm and 100 nm in diameter, superconductivity

was found under ambient pressure in 18 out of 38 samples. Careful transmission electron microscopy (TEM) studies revealed that the samples that exhibit superconductivity had a uniform granular morphology with all the rhombohedral Bi grains (~ 10 nm) aligned with a preferred orientation along the entire length of the wire. For the non-superconducting granular Bi samples, the rhombohedral Bi grains showed random orientation and both wire diameter and the grain size also showed considerable variations along the length of the wire. The superconductivity in the BiNW was attributed to small regions of high pressure Bi phase formed at the boundaries of partially aligned grains. These high pressure regions with the strained lattice probably cannot be detected by X-ray diffractometry because the strain regions are only a few atomic layers thick and do not contribute much to the signal from the sample.

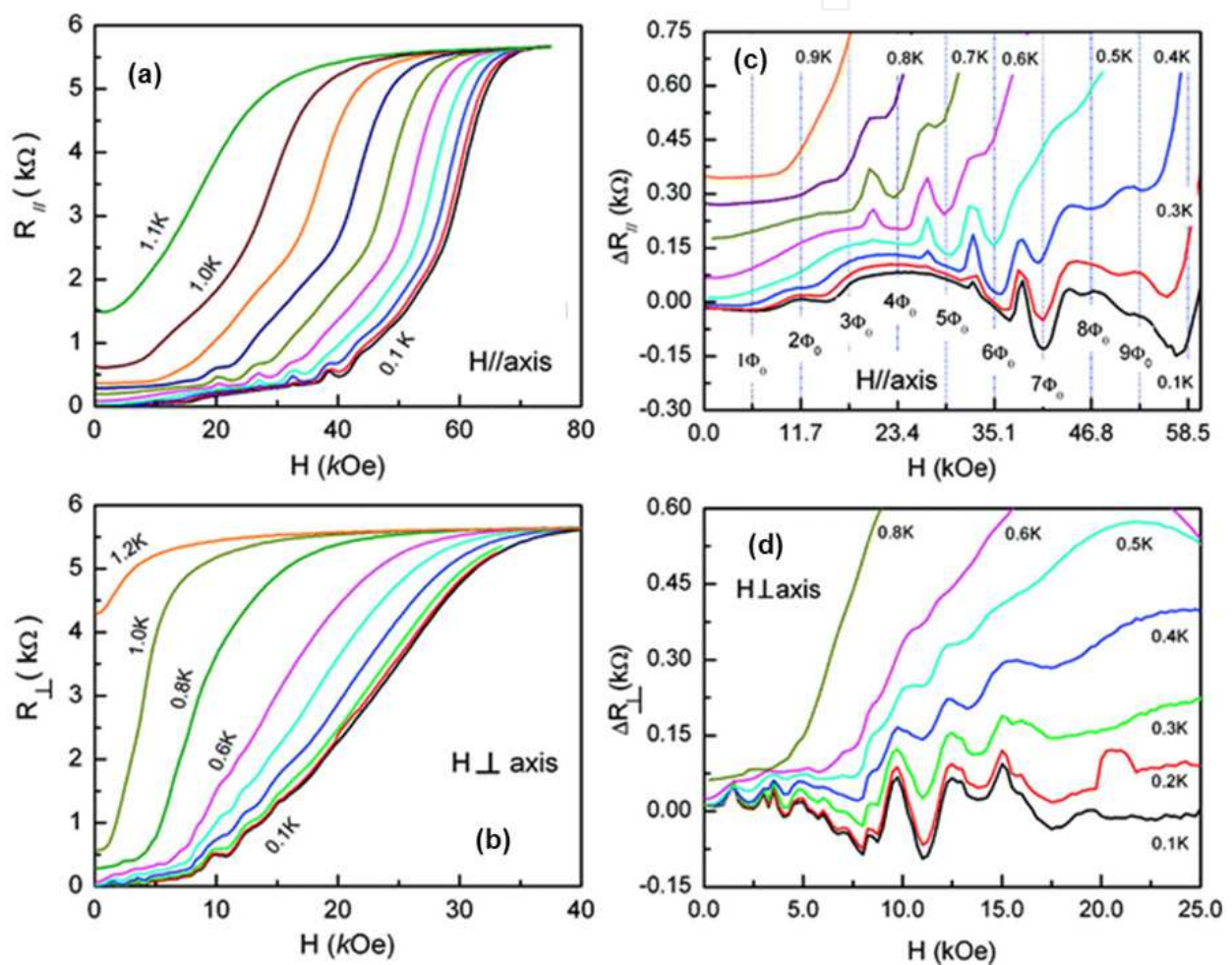


Fig. 13. (Tian et al., 2009) Resistance vs. applied magnetic field plots for a 79 nm diameter bismuth nanowire contacted with focused ion beam deposited normal platinum electrodes in a four-probe configuration at different temperatures for magnetic fields: (a) applied parallel to the wire axis; (b) applied perpendicular to the wire axis. (c) $\Delta R_{||}$ -H and (d) ΔR_{\perp} -H plots, obtained by subtracting smooth background from the data in Figures 13(a) and (b) respectively. Periodic oscillations of R were clearly seen in parallel H, and the dashed lines in panel (c) indicate the positions of fluxoid quantization as predicted by $H_{(\pi d^2/4)} = n\Phi_0$ with d = diameter of the nanowire = 67 nm. In perpendicular H, the R oscillations are more complex and their periodicity is with $1/H$.

Bi under high pressure is known to turn superconducting due to the formation of high-pressure metallic polymorphs, namely, monoclinic Bi-II at 2.55 GPa (Brugger et al., 1967; Degtyareva et al., 2004; Nédellec et al., 1974), a complex tetragonal Bi-III at 2.7 GPa (Degtyareva et al., 2004; Haussermann et al., 2002), and a body centered cubic (bcc) Bi-V at 7.7 GPa. (Chen et al., 1969; Degtyareva et al., 2004). The transition temperatures of these polymorphic phases are respectively 3.9, 7.2, and 8.3 K (Brandt & Ginzburg, 1969). T_c s of 8.3 K and 7.2 K are also seen in the superconducting transition of the granular BiNW further strengthening the idea that small regions of high pressure Bi phase exist in the nanowire. As discussed in the next paragraph, crystalline BiNW also remarkably displayed superconductivity with a T_c of 1.3 K.

In a recent experiment (Tian et al., 2009), quantum oscillations of the resistance as a function of applied field (H) were found in crystalline BiNW in a standard four-probe measurement with FIB deposited normal Pt electrodes. The crystalline BiNW were superconducting with a transition temperature of 1.3 K. In parallel field, below the critical field ($H_c \sim 7T$), a long resistance tail was present (figure 13(a)). On subtracting a uniform background from the resistance, and plotting the remainder ΔR_{\parallel} , the oscillations are clearly seen (figure 13 (c)). The oscillations are periodic with H and the period corresponds to the superconducting quantum flux ($\varphi_0 = h/2e = 2 \times 10^{-7} Gcm^2$). These oscillations are reminiscent of the Little-Parks (LP) oscillations caused by fluxoid quantization in hollow superconducting cylinders when the thickness of the shell is comparable to ξ (Little & Parks, 1962; Parks & Little, 1964). The standard LP oscillations in a small hollow cylinder are characterized by the integer multiples of the superconducting flux quantum, Φ_0 , that is, $H(\pi d^2/4) = n\Phi_0$, where d is the diameter of the hollow cylinder and n is an integer. Using this model, the period of the oscillations seen in BiNW, $\Delta H = 5.85$ kOe results in $d = 67.0$ nm. The diameter of the nanowire determined by TEM is 79 nm with a $\sim 3.7 \pm 0.5$ nm oxidation layer on the surface leaving the nanowire with an effective diameter of ~ 72 nm. This is close to the diameter calculated using LP oscillations. The LP-like oscillations unambiguously suggest that the observed superconductivity in BiNW originates from the cylindrical shell between the inner core of the Bi nanowire and its surface oxide.

When the field is aligned perpendicular to the wire axis, the residual resistance below 0.8 K still shows oscillations with varying H (figure 13(b)). On subtracting the residual resistance and plotting the remainder ΔR_{\perp} , (figure 13(d)), it is seen that these oscillations are periodic with $1/H$ rather than with H . The $1/H$ periodicity of the residual resistance oscillations is suggestive of the Shubnikov-de Haas (SdH) effect due to the Landau quantization of the conduction electrons in a metal. The SdH behavior in the superconducting state is not expected; therefore it is tempting to attribute it to the normal core. This explanation however, is not correct, because in the presence of a superconducting shell, the current will bypass the normal core and the normal core will not contribute to the resistance. In the paper (Tian et al., 2009) it is speculated that the SdH oscillations also originate from the superconducting shell. The finite residual resistance is a result of the phase slips in the shell. The normal region created in the shell because of these phase slips, behaves like a normal metal and shows SdH oscillations in the presence of a strong field. Both LP-like oscillations in parallel H and SdH-like oscillations in perpendicular H being observed in the same system suggest a completely unexpected and novel coexistence of superconducting and

metallic states in the surface shell of the Bi nanowire below T_c . The presence of superconductivity in ambient pressure BiNW is in itself a surprising result that brings to mind possibilities of other materials known to be non-superconducting in bulk showing superconductivity in the nanoscale. In addition, the fact that the superconductivity seems to be present only on the surface while the core continues to be normal, indicates that this superconductivity is an interface related phenomenon. The presence of SdH oscillations indicates metallic states on the surface. Metallic surface states are a prerequisite for the formation of a topological insulator (Fu et al., 2007). These new findings suggest that this old material may have potential application in developing next-generation quantum computing devices.

3.6 Pb nanobelts

Superconducting films on semiconductor substrates have attracted much attention since the derived superconductor-based electronics have been shown to be promising for future data processing and storage technologies. Current semiconductor technology is mainly based on silicon wafers. The superconductivity and applications of low dimensional Pb nanostructural superconductors have been extensively studied in recent decades (Wang et al., 2007, 2008a, 2008b, 2009b, 2009c, 2010b) because of the relatively higher transition temperature ($T_c \sim 7.2$ K) of bulk Pb compared to other conventional superconductors. The structure formed by two dimensional (2D) superconducting Pb films on Si substrate provides an excellent research system and has a wide application field. Qi-Kun Xue et al. have carried out a series of systematic experiments in high quality 2D single crystalline Pb film systems by utilizing scanning tunneling microscope (STM) and have achieved many outstanding results (Bao et al., 2005; Guo et al., 2004; T. Zhang et al., 2010; Y. F. Zhang et al., 2005). The Pb films are synthesized by using an MBE chamber. Based on previous work (Jalochowski et al., 1995; Upton et al., 2004), Q. K. Xue's group made great achievements in fabricating crystalline Pb films by MBE. They have made ultrathin Pb films from one atomic layer to tens of layers on Si (111) substrates. The Si substrate was firstly heated at 400°C for hours to get rid of the molecular gas absorbed at the surface, and then the substrate was flashed or annealed to ~1200°C several times to form a clean surface. After that, the substrate was cooled down to ~95 K by liquid nitrogen during growth to achieve atomically flat single crystal Pb thin films over a macroscopic area. By means of STM, scanning tunneling spectroscopy (STS), and transport measurements various intriguing properties of the 2D Pb systems have been discovered. These include "magic film thickness", "preferential island heights", "oscillating superconductivity transition temperatures" and other novel behaviors because of the strong quantum confinement effect (Bao et al., 2005; Eom et al., 2006; Guo, et al., 2004; Herzog et al., 1996; Markovic et al., 1998; Parendo et al., 2004; Xiong et al., 1997).

High quality Pb films are not only important for fundamental research, but also offer possibilities of electronic device fabrication. From the view point of applications, Pb films and related nanodevices have been predominantly prepared on semiconductor substrates. In recent years, J. Wang and his collaborators performed experiments on nanoscale systems based on Pb films grown on Si substrates (Wang et al., 2007, 2008a, 2008b, 2009b, 2009c, 2010b). In the Pb thin film with a unique fractal-like morphology grown on Si (111)-7×7

surface, the films exhibit distinctive negative magnetoresistance with wide magnetoresistance terrace under the perpendicular magnetic field. Analysis of the experimental results revealed that the observed effect originates from the coexistence of two superconducting phases in the system: the percolation structures with lower critical field (H_c) and the flat 2D Pb islands with higher H_c . In the low temperature regime, electron tunneling dominates the transport property of the percolation structures. When a magnetic field is applied, the superconducting gap is suppressed. Reducing the gap leads to a significant decrease of the resistance. The unusual magnetoresistance effect in the coexistence phase is of both fundamental interest and has possible applications in fabrication of hybrid devices based on the traditional microelectronics and the emerging superconducting quantum electronics (Leggett, 2002).

The high quality Pb films can also be etched to quasi-one dimensional (quasi-1D) single crystal Pb superconductor nanobridge (several nanometers thick and 100 to 500 nanometers wide) by using an FIB system (the measurement geometry are shown in figure 14). The Pb nanostructures thus formed were measured in a physical property measurement system (PPMS) with standard four-electrode method. Many interesting phenomena with the different widths and thicknesses of the Pb nanobridges were observed by studying the transport properties, such as the enhanced superconductivity (T_C) compared to the film with the same thickness (Wang et al., 2008a), magnetoresistance (MR) oscillations (Wang et al., 2008a, 2009c, 2010b), the broadening of the transition near T_C because of thermally activated phase-slip (TAPS), multiple voltage steps, and power-law Voltage vs. Current relationship (Wang et al., 2009b). The properties and the unique structures provide a new approach for integrating superconducting circuits on single Si chips, for example nanoscale SQUID-like devices (Johansson et al., 2005), "on-off" functional and logical nanodevices.

Furthermore, atomically uniform single-crystal epitaxial Pb films, several nanometers thick, were fabricated on a Si substrate to form a sharp superconductor-semiconductor heterojunction (SSH) by FIB etching (Wang et al., 2008b) as shown in figures 15 (a) and (b). The transport measurements of the junction showed an unusual magnetoresistance effect when the Pb film was superconducting. The resistance of the SSH decreased sharply with increasing magnetic field and was very sensitive to the temperature below T_C (figure 15 (c)). Such sensitivity and the SSH structure make the Pb-Si junction highly promising for mass production for use in developing a magnetic field controlled "on-off" device and new cryogenic temperature detectors on Si chips (Day et al., 2003; Irwin et al., 1996). The devices derived by superconductor films on semiconductor substrates have many promising applications in the future.

The giant magnetoresistance (GMR) effect was discovered in the late 1980s on Fe/Cr magnetic multilayer (Baibich et al., 1988) and Fe/Cr/Fe tri-layers (Binasch et al., 1989). It was seen that as the applied field was increased, the resistance of the multilayer structure decreased (6% for Fe/Cr/Fe tri-layers and 50% for Fe/Cr magnetic multilayer, respectively). This discovery was significant to the scientific community and caught widespread attention in the industry. The researchers of IBM recognized its potential and invented spin-valves (Tsang et al., 1994) and the commercial read head was created (Wolf et al., 2001). GMR's application in the read head of hard discs greatly increases the density of stored information. Since the introduction of GMR-type sensors as reading elements, storage capacities have increased approximately 100 times (Grunberg, 2008). Moreover, magnetic random access memory (MRAM), medical/biological sensors and various logic components

have been invented by using the GMR effect. Meanwhile, GMR is often viewed as the founding stone of spintronics, where the electron spin is the key to physical functionality. Thus GMR of the magnetic multilayers opened the way to an efficient control of the motion of the electrons by acting on their spin through the orientation of a magnetization. In the SSH composed of Pb/Si system, described in the paragraph above, J. Wang and his collaborators observed a dramatic negative magnetoresistive effect (Wang et al., 2008b). Compared to the Fe/Cr magnetic multilayer in 1988 (Baibich et al., 1988), the resistance changes more with increasing the magnetic field, and the saturated critical field of the SSH is smaller than that of Fe/Cr multilayer by an order at the same temperature.

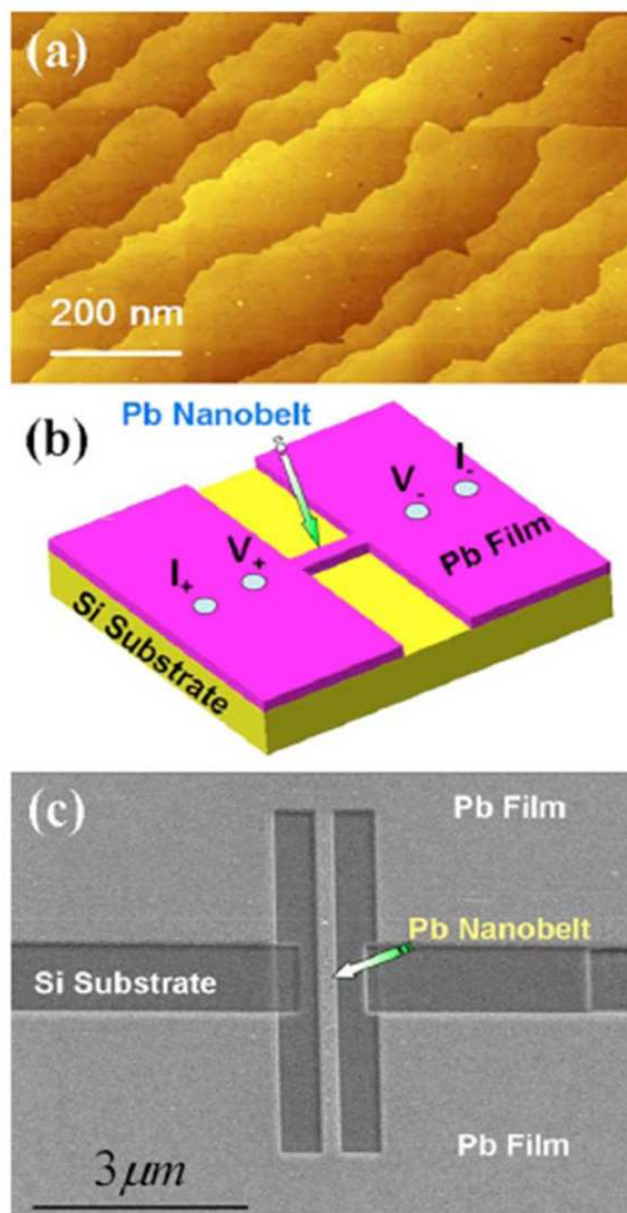


Fig. 14. (Wang et al., 2008b) (a) A scanning tunneling microscope image of the atomically smooth lead thin film on the Si(111) 7×7 substrate. (b) The schematic graph for the transport measurement across the lead nanobelt. (c) A SEM image of the lead nanobelt made by milling the lead film.

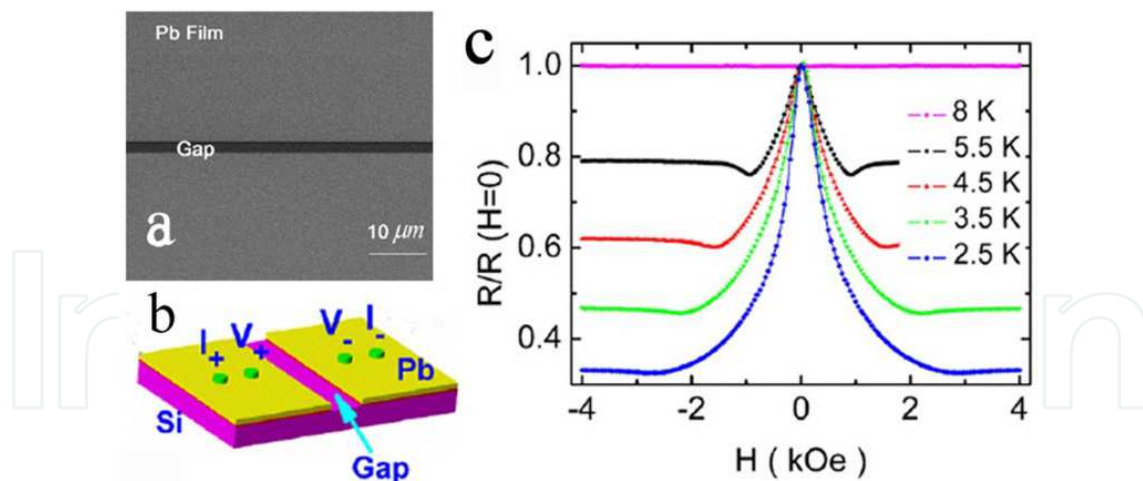


Fig. 15. (Wang et al., 2008b) (a) A scanning electron micrograph of the Pb film after a $2\mu\text{m}$ wide gap (the dark region) was fabricated. (b) The schematic graph for the transport measurement across the Pb/Si (111) heterojunctions. (c) Magnetoresistance of the heterojunctions with a magnetic field perpendicular to the film at different temperatures. The vertical scale is normalized to the resistance at zero magnetic field.

Although the physical mechanisms in traditional GMR and the giant negative magnetoresistive effect in SSH are completely different and the resistance changes in SSH only happens at low temperatures, it is reasonable to believe that the large magnetoresistance effect in SSH may also be extended and applied in technology and other fields such as magnetic switches, temperature or magnetic field sensors, high-density information storage and quantum computing circuits. It is to be remembered that Pb is a metal and is easily oxidized in atmosphere. Therefore, cover layers of Ge, Si, Au etc. need to be used to protect Pb based devices for applications.

3.7 Josephson effect and superconducting quantum interference device (SQUID)

A Josephson junction is composed of two superconducting layers coupled by a weak link. The weak link can consist of a thin insulating barrier (S-I-S), a short section of non-superconducting metal (S-N-S), or a physical constriction that weakens the superconductivity at the point of contact (S-c-S). The Josephson Effect is the phenomenon that the current can tunnel through the junction (or weak link) without any voltage applied (Josephson, 1962, 1974). It was observed by the British physicist B. D. Josephson, who was the first to predict the tunneling of superconducting Cooper pairs (before that, it was only known that normal electrons can tunnel through an insulating barrier). Josephson received the Nobel prize in 1973 for this finding. Josephson junctions have important applications in superconducting quantum interference devices (SQUID), single-electron transistors, superconducting qubits and rapid single flux quantum (RSFQ) digital electronics. SQUID is a very sensitive magnetometer used to measure extremely weak magnetic fields (Range, 2002), based on superconducting loops containing one or two Josephson junctions. For instance, the SQUID magnetometer reaches $7 \times 10^{-11} \text{ Os/Hz}^{1/2}$ which is higher than that of the best traditional magnetometer by one order. SQUID is used as a sensitive sensor that can detect the tiny magnetic flux changes through measuring the other visible parameters. It can be used in many fields.

The most common use of SQUID is probably in magnetic property measurement systems (MPMS). The SQUID is being used as a detector to perform MRI because of its extreme sensitivity. It is an ideal device for studying biological systems. In the clinical environment, the applications of SQUID are wide. For example, Magnetoencephalography (MEG) (Cohen, 1972), which is an equipment that measures and traces the extremely weak biomagnetic signals emitted by the brain. The SQUID is also used in cardiology for magnetic field imaging (MFI) (Brockmeier et al., 1994), which detects the magnetic field of the heart for diagnosis and risk stratification. In the other fields of biology, SQUID also plays a significant role such as recording the weak magnetic fields of the stomach, tracing the path of orally applied drugs in human body. Additionally, in geological exploration, the SQUID-superconducting magnetic magnetometer can be used to measure the geomagnetic field accurately and analyze the distribution to observe the valuable mineral deposits. For earthquake prediction, it can be used to detect the gravity changes on a floating superconducting ball. The changes in gravity change the relative position of the ball and the superconducting ring and cause distortion of the magnetic field. The changing magnetic field can be detected by SQUID-Gravimeter (Verkin et al., 1976). Furthermore, it is also promising as a potential component in quantum computers (Bouchiat et al., 1998) and in precision sensors. The applications of SQUID are many.

With the development of semiconductor industry, electronic devices are rapidly becoming smaller. Although the sensitivity of the SQUID increases with the area of the superconducting ring, nano-SQUID is also needed for detecting the weak magnetic signals of small structures and integrating the logic components of computers. The British "New Scientist" magazine reported (Troeman et al., 2007) that researchers in Holland had fabricated the smallest SQUID in the world. It is 180 nm in diameter and was made by Nb. To maintain superconductivity of the device, the whole system needs to operate at low temperatures. Pb also has T_C higher than liquid helium temperature and is suitable for work in helium cooling conditions. In addition, the possibility of using focused ion beam and electron beam lithography techniques discussed in this chapter on silicon substrate offers the possibility of synthesizing millions or billions of SQUIDs devices in one chip.

4. Conclusion

Superconductivity and its applications in science and technology is currently one of the most important research fields. In recent decades, the developments in this field have been extremely rapid and superconductors are extensively used in many applications. With the dimensions of electronic circuits reduced to nanometer scale, it becomes important to study the physics of superconductivity on this scale for potential nano-superconducting circuit elements. Many interesting properties are exhibited in superconducting nanowires with various morphologies, which offer numerous opportunities for applications.

The interesting physics observed in nanowires and nanobelts discussed in the chapter proves that they are an ideal platform for helping in understanding the fundamental nature of superconductivity. Furthermore, the plethora of synthesis techniques available, offer flexibility in morphology and performance control. The very high quality, defect free nanostructures like Pb films discussed in the chapter are ideal candidates for studying low-dimensional superconductivity because they enable the separation of true low-dimensional

physics from the effects caused due to defects and morphology. It is also possible to fabricate such devices for use in integrated circuits on Si substrates. The e-beam lithography technique used for gold, aluminum and lead nanobelts is especially suitable for this. Examples like nano-squid and single-electron transistors (Fulton & Dolan, 1987) enabling extremely sensitive magnetic field and charge measurements demonstrate the tremendous potential for applications of nanoscale superconducting devices. The factor limiting widespread use of these devices is still the low temperatures required and the prohibitive cost of the helium needed to reach those low temperatures. Much research has been done to achieve usable high T_c superconductors. However, till now, high temperature superconductors have realized applications only in very limited fields. Although their T_c is higher than conventional metallic superconductors, they are ceramic, making them inflexible and hard to machine compared to metallic superconductors. The low T_c of metallic superconductors, limiting their applications in devices, is not a problem in potential applications to space technology (ambient temperature in space $\sim 3K$ and many metallic superconductors have T_c higher than this). Due to properties like high speed (response rate is 10-100 times faster than conventional devices), ultra-low noise (the thermal noise is much lower than conventional semiconductor devices) and low heat dissipation, superconductivity in aerospace applications such as space communications, radar guidance etc. is widely used.

In summary, the use of superconducting nanoscale components will produce denser and more rapid chips since the resistance is a major source of heat generation and charging time in integrated circuits. Studying and understanding superconductivity on this scale is of great interest and importance.

5. Acknowledgement

We are grateful to Professors Moses H. W. Chan, Mingliang Tian, Qi-Kun Xue, Jainendra K. Jain, Thomas E. Mallouk, Nitin Samarth and Xu-Cun Ma for the collaboration in this project. This work was financially supported by the National Natural Science Foundation of China (No. 11174007) and National Basic Research Program (NBRP) of China (No. 2012CB921300), the Penn State MRSEC under NSF grant DMR-0820404, and China Postdoctoral Science Foundation (No. 2011M500180).

6. References

- Altomare, F., Chang, A. M., Melloch, M. R., Hong, Y. G., & Tu, C. W. (2006). Evidence for Macroscopic Quantum Tunneling of Phase Slips in Long One-dimensional Superconducting Al Wires. *Physical Review Letters*, Vol. 97, No. 1, (July 2006), pp. (017001), ISSN 0031-9007
- Arthur, J. R. (2002). Molecular Beam Epitaxy. *Surface Science*, Vol. 500, No. 1-3, (March 2002), pp. (189-217), ISSN 0039-6028
- Aumentado, J., & Chandrasekhar, V. (2001). Mesoscopic Ferromagnet-Superconductor Junctions and the Proximity Effect. *Physical Review B*, Vol. 64, No. 5, (August 2001), pp. (054505), ISSN 0163-1829
- Baibich, M. N., Broto, J. M., Fert, A., Vandau, F. N., Petroff, F., Eitenne, P., Creuzet, G., Friederich, A., & Chazelas, J. (1988). Giant Magnetoresistance of (001)Fe/(001)Cr

- Magnetic Superlattices. *Physical Review Letters*, Vol. 61, No. 21, (November 1988), pp. (2472-2475), ISSN 0031-9007
- Bao, X. Y., Zhang, Y. F., Wang, Y. P., Jia, J. F., Xue, Q. K., Xie, X. C., & Zhao, Z. X. (2005). Quantum Size Effects on the Perpendicular Upper Critical Field in Ultrathin Lead Films. *Physical Review Letters*, Vol. 95, No. 24, (December, 2005), pp. (247005), ISSN 0031-9007
- Bera, D., Kuiry, S. C., & Seal, S. (2004). Synthesis of Nanostructured Materials using Template-assisted Electrodeposition. *JOM*, Vol. 56, No. 1, (January 2004), pp. (49-53), ISSN 1047-4838
- Bergeret, F. S., Volkov, A. F., & Efetov, K. B. (2005). Odd Triplet Superconductivity and Related Phenomena in Superconductor-Ferromagnet Structures. *Reviews of Modern Physics*, Vol. 77, No. 4, (October 2005), pp. (1321-1373), ISSN 0034-6861
- Bezryadin, A., Lau, C. N., & Tinkham, M. (2000). Quantum Suppression of Superconductivity in Ultrathin Nanowires. *Nature*, Vol. 404, No. 6781, (April 2000), pp. (971-974), ISSN 0028-0836
- Binasch, G., Grunberg, P., Saurenbach, F., & Zinn, W. (1989). Enhanced Magnetoresistance in Layered Magnetic-Structures with Antiferromagnetic Interlayer Exchange. *Physical Review B*, Vol. 39, No. 7, (March 1989), pp. (4828-4830), ISSN 1098-0121
- Bouchiat, V., Vion, D., Joyez, P., Esteve, D., & Devoret, M. H. (1998). Quantum Coherence with Single Cooper Pair. *Physica Scripta*, Vol. T76, (January 1998), pp. (165-170), ISSN 0281-1847
- Brandt, N. B., & Ginzburg, N. I. (1969). Superconductivity at High Pressures. *Contemporary Physics*, Vol. 10, No. 4, (April 1969), pp. (355-384), ISSN 0010-7514
- Brockmeier, K., Comani, S., Erne, S. N., Diluzio, S., Psquarelli, A., & Romani G. L. (1994). Magnetocardiography and Exercise Training. *Journal of Electrocardiology*, Vol. 27, No. 2, (April 1994), pp. (137-142), ISSN 0022-0736
- Brugger, R. M., Bennion, R. B., & Worlton, T. G. (1967). Crystal Structure of Bismuth-2 at 26 Kbar. *Physcs Letters A*, Vol. A24, No. 13, (June 1967), pp. (714-717), ISSN 0375-9601
- Chen, T. T., Chen, J. T., Leslie, J. D., & Smith, H. J. T. (1969). Phonon Spectrum of Superconducting Amorphous Bismuth and Gallium by Electron Tunneling. *Physical Review Letters*, Vol. 22, No. 11, (March 1969), pp. (526-530), ISSN 0031-9007
- Chen, Y., Snyder, S. D., & Goldman A. M. (2009). Magnetic-field-induced Superconducting State in Zn Nanowires Driven in the Normal State by an Electric Current. *Physical Review Letters*, Vol. 103, No. 12, (September 2009), pp. (127002), ISSN 0031-9007
- Chen, Y., Lin, Y. H., Snyder, S. D., & Goldman A. M. (2011). Stabilization of Superconductivity by Magnetic Field in Out-of-equilibrium Nanowires. *Physical Review B*, Vol. 83, No. 5, (February 2011), pp. (054505), ISSN 1098-0121
- Chiang, Y. N., Shevchenko, O. G., & Kolenov, R. N. (2007). Manifestation of Coherent and Spin-dependent Effects in the Conductance of Ferromagnets Adjoining a Superconductor. *Low Temperature Physics*, Vol. 33, No. 4, (April 2007), pp. (314-320), ISSN 1063-777X
- Cohen, D. (1972). Magnetoencephalography - Detection of Brains Electrical-activity with a Superconducting Magnetometer. *Science*, Vol. 175, No. 4022, (February 1972), pp. (664-666), ISSN 0036-8075

- Day, P. K., LeDuc, H. G., Mazin, B. A., Vayonakis, A., & Zmuidzinas, J. (2003). A Broadband Superconducting Detector Suitable for Use in Large Arrays. *Nature*, Vol. 425, No. 6960, (October 2003), pp. (817-821), ISSN 0028-0836
- Degtyareva, O., McMahon, M. I., & Nelmes, R. J. (2004). High-pressure Structural Studies of Group-15 Elements. *High Pressure Research*, Vol. 24, No. 3, (September 2004), pp. (319-356), ISSN 0895-7959
- Eom, D., Qin, S., Chou, M. Y., & Shih, C. K. (2006). Persistent Superconductivity in Ultrathin Pb Films: A Scanning Tunneling Spectroscopy Study. *Physical Review Letters*, Vol. 96, No. 2, (January, 2006), pp. (027005), ISSN 0031-9007
- Eschrig, M. (2011). Spin-polarized Supercurrents for Spintronics. *Physics Today*, Vol. 64, No. 1, (January 2011), pp. (43-49), ISSN 0031-9228
- Fu, H. C., Seidel, A., Clarke, J., & Lee, D. (2006). Stabilizing Superconductivity in Nanowires by Coupling to Dissipative Environments. *Physical Review Letters*, Vol. 96, No. 15, (April 2006), pp. (157005), ISSN 0031-9007
- Fu, L., Kane, C. L., & Mele, E. J. (2007). Topological Insulators in Three Dimensions. *Physical Review Letters*, Vol. 98, No. 10, (March, 2007), pp. (106803), ISSN 0031-9007
- Fulton, T. A., & Dolan, G. J. (1987). Observation of single-electron charging effects in small tunnel junctions. *Physical Review Letters*, Vol. 59, No. 1, (July, 1987), pp. (109-112), ISSN 0031-9007
- Giordano, N. (1988). Evidence for Macroscopic Quantum Tunneling in One-dimensional Superconductors. *Physical Review Letters*, Vol. 61, No. 18, (October 1988), pp. (2137-2140), ISSN 0031-9007
- Giordano, N., & Schuler, E. R. (1990). Giant Conductance Fluctuations in Thin Metal Wires. *Physical Review B*, Vol. 41, No. 17, (June 1990), pp. (11822-11826), ISSN 0163-1829
- Giordano, N. (1991). Superconductivity and Dissipation in Small-diameter Pb-In Wires. *Physical Review B*, Vol. 43, No. 1, (January 1991), pp. (160-174), ISSN 0163-1829
- Giordano, N. (1994). Superconducting Fluctuations in One-dimension. *Physica B*, Vol. 203, No. 3-4, (December 1994), pp. (460-466), ISSN 0921-4526
- Giroud, M., Courtois, H., Hasselbach, K., Mailly, D., & Pannetier, B. (1998). Superconducting Proximity Effect in a Mesoscopic Ferromagnetic Wire. *Physical Review B*, Vol. 58, No. 18, (November 1998), pp. (11872-11875), ISSN 1098-0121
- Grunberg, P. A. (2008). Nobel Lecture: From Spin Waves to Giant Magnetoresistance and Beyond. *Reviews of Modern Physics*, Vol. 80, No. 4, (October - December 2008), pp. (1531-1540), ISSN 0034-6861
- Guo, Y., Zhang, Y. F., Bao, X. Y., Han, T. Z., Tang, Z., Zhang, L. X., Zhu, W. G., Wang, E. G., Niu, Q., Qiu, Z. Q., Jia, J. F., Zhao, Z. X., & Xue, Q. K. (2004). Superconductivity Modulated by Quantum Size Effects. *Science*, Vol. 306, No. 5703, (December, 2004), pp. (1915-1917), ISSN 0036-8075
- Gupta, A. K., Cretinon, L., Moussy, N., Pannetier, B., & Courtois, H. (2004). Anomalous Density of States in a Metallic Film in Proximity with a Superconductor. *Physical Review B*, Vol. 69, No. 10, (March, 2004), pp. (104514), ISSN 1098-0121
- Hartman, R. (1969). Temperature Dependence of Low-field Galvanomagnetic Coefficients of Bismuth. *Physical Review*, Vol. 181, No. 3, (May, 1969), pp. (1070-1086), ISSN 0031-899X

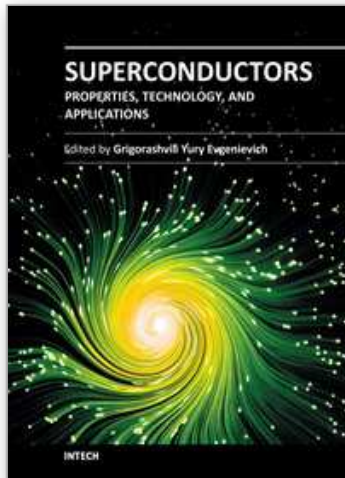
- Haussermann, U., Soderberg, K., & Norrestarrit, R. (2002). Comparative Study of the High-pressure Behaviour of As, Sb and Bi. *Journal of the American Chemical Society*, Vol. 124, No. 51, (December, 2002), pp. (15359-15367), ISSN 0002-7863
- He, L., & Wang, J. (2011). Periodic Magnetoresistance Oscillations Induced by Superconducting Vortices in Single Crystalline Au Nanowires. *Nanotechnology*, Vol. 22, No. 44, (September, 2011), pp. (445704), ISSN 1361-6528
- Herzog, A. V., Xiong, P., Sharifi, F., & Dynes R. C. (1996). Observation of a Discontinuous Transition from Strong to Weak Localization in 1D Granular Metal Wires. *Physical Review Letters*, Vol. 76, No. 4, (January, 1996), pp. (668-671), ISSN 0031-9007
- Herzog, A. V., Xiong, P., & Dynes R. C. (1998). Magnetoresistance Oscillations in Granular Sn Wires Near the Superconductor-Insulator Transition. *Physical Review B*, Vol. 58, No. 21, (December 1998), pp. (14199-14202), ISSN 0163-1829
- Hohenberg, P. C. (1967). Existence of Long-Range Order in 1 and 2 Dimensions. *Physical Review*, Vol. 158, No. 2, (June 1967), pp. (383-386), ISSN 0031-899X
- Irwin, K. D., Hilton, G. C., Wollman, D. A., & Martinis, J. M. (1996). X-Ray Detection Using a Superconducting Transition-edge Sensor Microcalorimeter with Electrothermal Feedback. *Applied Physics Letters*, Vol. 69, No. 13, (September 1996), pp. (1945-1947), ISSN 0003-6951
- Jalochowski, M., Hoffmann, M., & Bauer, E. (1995). Pb Layer-by-layer Growth at Very-low Temperatures. *Physical Review B*, Vol. 51, No. 11, (March 1995), pp. (723-7238), ISSN 1098-0121
- Johansson, A., Sambandamurthy, G., Shahar, D., Jacobson, N., & Tenne, R. (2005). Nanowire Acting as a Superconducting Quantum Interference Device. *Physical Review Letters*, Vol. 95, No. 11, (September 2005), pp. (116805), ISSN 0031-9007
- Josephson, B. D. (1962). Possible New Effects in Superconductive Tunneling. *Physics Letters*, Vol. 1, No. 7, (July 1962), pp. (251-253)
- Josephson, B. D. (1974). Discovery of Tunneling Supercurrents. *Reviews of Modern Physics*, Vol. 46, No. 2, (April, 1974), pp. (251-254), ISSN 0034-6861
- Keizer, R. S., Goennenwein, S. T. B., Klapwijk, T. M., Miao, G. X., Xiao, G., & Gupta, A. (2006). A Spin Triplet Supercurrent through a Half-metallic Ferromagnet CrO₂. *Nature*, Vol. 439, No. 7078, (February 2006), pp. (825-827), ISSN 0028-0836
- Khaire, T. S., Khasawneh, M. A., Pratt, W. P., & Birge, N. O. (2010). Observation of Spin-Triplet Superconductivity in Co-Based Josephson Junctions. *Physical Review Letters*, Vol. 104, No. 13, (April 2010), pp. (137002), ISSN 0031-9007
- Knoedler, C. M. (1990). Helium-ion Damage and Nanowire Fabrication in GaAs/AlGaAs Heterostructures. *Journal of Applied Physics*, Vol. 68, No. 3, (August 1990), pp. (1129-1137), ISSN 0021-8979
- Konschelle, F., Cayssol, J., & Buzdin, A. (2010). Long-range Singlet Proximity Effect in Ferromagnetic Nanowires. *Physical Review B*, Vol. 82, No. 18, (November 2011), pp. (180509), ISSN 1098-0121
- Langer, J. S., & Ambegaokar, V. (1967). Intrinsic Resistive Transition in Narrow Superconducting Channels. *Physical Review*, Vol. 164, No. 2, (December 1967), pp. (498-510), ISSN 0031-899X
- Lau, C. N., Markovic, N., Bockrath, M., Bezryadin, A., & Tinkham, M. (2001). Quantum Phase Slips in Superconducting Nanowires. *Physical Review Letters*, Vol. 87, No. 21, (November 2001), pp. (217003), ISSN 0031-9007

- Lee, W., Ji, R., Gosele, U., & Nielsch, K. (2006). Fast Fabrication of Long-range Ordered Porous Alumina Membranes by Hard Anodization. *Nature Materials*, Vol. 5, No. 9, (September 2006), pp. (741-747), ISSN 1476-1122
- Leggett, A. J. (2002). Physics - Superconducting Qubits - A Major Roadblock Dissolved?. *Science*, Vol. 296, No. 5569, (May 2002), pp. (861-862), ISSN 0036-8075
- Le Sueur, H., Joyez, P., Pothier, H., Urbina, C., & Esteve, D. (2008). Phase Controlled Superconducting Proximity Effect Probed by Tunneling Spectroscopy. *Physical Review Letters*, Vol. 100, No. 19, (May 2008), pp. (197002), ISSN 0031-9007
- Little, W. A., & Parks, R. D. (1962). Observation of Quantum Periodicity in Transition Temperature of a Superconducting Cylinder. *Physical Review Letters*, Vol. 9, No. 1, (June 1962), pp. (9-12), ISSN 0031-9007
- Liu, Y., & Allen, R. (1995). Electronic-structure of the Semimetals Bi and Sb. *Physical Review B*, Vol. 52, No. 3, (July, 1995), pp. (1566-1577), ISSN 0163-1829
- Lucignano, P., Stornaiuolo, D., Tafuri, F., Altshuler, B. L., & Tagliacozzo, A. (2010). Evidence for a Minigap in BCO Grain Boundary Josephson Junctions. *Physical Review Letters*, Vol. 105, No. 14, (September 2010), pp. (147001), ISSN 0031-9007
- Madou, M. J. (2002). *Fundamentals of Microfabrication: The Science of Miniaturization* (2nd edition), CRC Press, ISBN 0-8493-0826-7, USA
- Markovic, N., Mack, A. M., Martinez-Arizala, G., Christiansen, C., & Goldman, A. M. (1998). Evidence of Vortices on the Insulating Side of the Superconductor-Insulator Transition. *Physical Review Letters*, Vol. 81, No. 3, (July 1998), pp. (701-704), ISSN 0031-0097
- McCumber, D. E., Halperin, B. I. (1970). Time Scale of Intrinsic Resistive Fluctuations in Thin Superconducting Wires. *Physical Review B*, Vol. 1, No. 3, (February, 1970), pp. (1054-1070)
- Menon, V. P., & Martin, C. R. (1995). Fabrication and Evaluation of Nanoelectrode Ensembles. *Analytical Chemistry*, Vol. 67, No. 13, (July 1995), pp. (1920-1928), ISSN 0003-2700
- Mermin, N. D., & Wagner, H. (1966). Absence of Ferromagnetism or Antiferromagnetism in one- or 2-dimensional Isotropic Heisenberg Models. *Physical Review Letters*, Vol. 17, No. 22, (November 1966), pp. (1133-1136), ISSN 0031-9007
- Mooij, J. E., Harmans, C. J. P. (2005). Phase-slip Flux Qubits. *New Journal of Physics*, Vol. 7, (October 2005), pp. (219), ISSN 1367-2630
- Nédellec, P., Dumoulin, L., & Noer, R. J. (1974). Electron Tunneling Study of Superconducting High-pressure Phase of Bi. *Journal of Physics F*, Vol. 4, No. 6, (June, 1974), pp. (L145-L150), ISSN 0305-4608
- Nielsch, K., Castano, F. J., Matthias, S., Lee, W., Ross, C. A. (2005). Synthesis of Cobalt/Polymer Multilayer Nanotubes. *Advanced Engineering Materials*, Vol. 7, No. 4, (April 2005), pp. (217-221), ISSN 1438-1656
- Parendo, K. A., Hernandez, L. M., Bhattacharya, A., & Goldman, A. M. (2004). Anomalous Parallel-field Negative Magnetoresistance in Ultrathin Films Near the Superconductor-insulator Transition. *Physical Review B*, Vol. 70, No. 21, (December, 2004), pp. (212510), ISSN 1098-0121
- Parks, R. D., & Little, W. A. (1964). Fluxoid Quantization in Multiply-connected Superconductor. *Physical Review*, Vol. 133, No. 1A, (January, 1964), pp. (A97-A103), ISSN 0031-899X

- Pena, V., Sefrioui, Z., Arias, D., Leon, C., Santamaria, J., Varela, M., Pennycook, S. J., & Martinez, J. L. (2004). Coupling of Superconductors through a Half-metallic Ferromagnet: Evidence for a Long-range Proximity Effect. *Physical Review B*, Vol. 69, No. 22, (June 2004), pp. (224502), ISSN 1098-0121
- Peng H. L., Kai, K. J., Kong, D. S., Meister, S., Chen, Y. L., Qi, X. L., Zhang, S. C., Shen, Z. X., & Cui, Y. (2010). Aharonov-Bohm Interference in Topological Insulator Nanoribbons. *Nature Materials*, Vol. 9, No. 3, (March 2010), pp. (225-229), ISSN 1476-1122
- Petrashov, V. T., Sosnin, I. A., Cox, I., Parsons, A., & Troadec, C. (1999). Giant Mutual Proximity Effects in Ferromagnetic/Superconducting Nanostructures. *Physical Review Letters*, Vol. 83, No. 16, (October 1999), pp. (3281-3284), ISSN 0031-9007
- Range, S. K. (2002). Balancing relevancy and accuracy: Presenting gravity probe B's science meaningfully, *Proceedings of NASA OSS Conference on Education and Public Outreach*, 1-58381-181-8, Chicago (USA), June 2002
- Reguera, G., McCarthy, K. D., Mehta, T., Nicoll, J. S., Tuominen, M. T., & Lovley, D. R. (2005). Extracellular electron transfer via microbial nanowires. *Nature*, Vol. 435, No. 7045, (June 2005), pp. (1008-1101), ISSN 0028-0836
- Rogachev, A., Wei, T. C., Pekker, D., Bollinger, A. T., Goldbart, P. M., & Bezryadin, A. (2006). Magnetic-field Enhancement of Superconductivity in Ultranarrow Wires. *Physical Review Letters*, Vol. 97, No. 13, (September 2006), pp. (137001), ISSN 0031-9007
- Santhanam, P., Chi, C. C., Wind, S. J., Brady, M. J., & Bucchignano, J. J. (1991). Resistance Anomaly near the Superconducting Transition-temperature in Short Aluminum Wires. *Physical Review Letters*, Vol. 66, No. 17, (April 1991), pp. (2254-2257), ISSN 0031-9007
- Sazio, P. J. A., Amezcua-Correa, A., Finlayson, C. E., Hayes, J. R., Scheidemantel, T. J., Baril, N. F., Jackson, B. R., Won, D. J., Zhang, F., Margine, E. R., Gopalan, V., Crespi, V. H., Badding, J. V. (2006). Microstructured Optical-fibers as High-pressure Microfluidic Reactors. *Science*, Vol. 311, No. 5767, (March 2006), pp. (1583-1586), ISSN 0036-8075
- Singh, M., Wang, J., Tian, M. L., Zhang, Q., Pereira, A., Kumar, N., Mallouk, T. E., & Chan, M. H. W. (2009). *Chemistry of Materials*, Vol. 21, No. 23, (December, 2009), pp. (5557-5559), ISSN 0897-4756
- Singh, M., Wang, J., Tian, M. L., Mallouk, T. E., & Chan, M. H. W. (2011). Antiproximity Effect in Aluminum Nanowires with no Applied Magnetic Field. *Physical Review B*, Vol. 83, No. 22, (June, 2011), pp. (220506), ISSN 1098-0121
- Sosnin, I., Cho, H., Petrashov, V. T., & Volkov, A. F. (2006). Superconducting Phase Coherent Electron Transport in Proximity Conical Ferromagnets. *Physical Review Letters*, Vol. 96, No. 15, (April 2006), pp. (157002), ISSN 0031-9007
- Stoltenberg, R. M., & Woolley, W. T. (2004). DNA-templated Nanowire Fabrication. *Biomedical Microdevices*, Vol. 6, No. 2, (June 2004), pp. (105-111), ISSN 1387-2176
- Tian, M. L., Wang, J. G., Snyder, J., Kurtz, J., Liu, Y., Schiffer, P., Mallouk, T. E., & Chan, M. H. W. (2003). Synthesis and Characterization of Superconducting Single-crystal Sn Nanowires. *Applied Physics Letters*, Vol. 83, No. 8, (August 2003), pp. (1620-1622), ISSN 0003-6951

- Tian, M. L., Kumar, N., Xu, S. Y., Wang, J. G., Kurtz, J. S., & Chan, M. H. W. (2005). Suppression of Superconductivity in Zinc Nanowires by Bulk Superconductors. *Physical Review Letters*, Vol. 95, No. 7, (August 2005), pp. (076802), ISSN 0031-9007
- Tian, M. L., Kumar, N., Wang, J. G., Xu, S. Y., & Chan, M. H. W. (2006a). Influence of a Bulk Superconducting Environment on the Superconductivity of One-dimensional Zinc Nanowires. *Physical Review B*, Vol. 74, No. 1, (July 2006), pp. (014515), ISSN 1098-0121
- Tian, M. L., Wang, J. G., Kumar, N., Tianheng, H., Kobayashi, Y., Liu, Y., Mallouk, T. E., & Chan, M. H. W. (2006b). Observation of Superconductivity in Granular Bi Nanowires Fabricated by Electrodeposition. *Nano Letters*, Vol. 6, No. 12, (November 2006), pp. (2773-2780), ISSN 1530-6984
- Tian, M. L., Wang, J., Zhang, Q., Kumar, N., Mallouk, T. E., & Chan, M. H. W. (2009). Superconductivity and Quantum Oscillations in Crystalline Bi Nanowire. *Nano Letters*, Vol. 9, No. 9, (September 2009), pp. (3196-3202), ISSN 1530-6984
- Troeman, A. G. P., Derking, H., Borger, B., Pleikies, J., Veldhuis, D., & Hilgenkamp, H. (2007). NanoSQUIDS Based on Niobium Constrictions. *Nano Letters*, Vol. 7, No. 7, (July 2007), pp. (2152-2156), ISSN 1530-6984
- Tsang, C., Fontana, R. E., Lin, T., Heim, D. E., Speriosu, V. S., Gurney, B. A., & Mason, M. L. (1994). Design, Fabrication and Testing of Spin-valve Read Heads for High-density Recording. *IEEE Transactions on Magnetics*, Vol. 30, No. 6, (November 1994), pp. (3801-3806), ISSN 0018-9464
- Upton, M. H., Wei, C. M., Chou, M. Y., Miller, T., & Chiang, T. C. (2004). Thermal Stability and Electronic Structure of Atomically Uniform Pb Films on Si(111). *Physical Review Letters*, Vol. 93, No. 2, (July 2004), pp. (026802), ISSN 0031-9007
- Verkin, B. I., Mende, F. F., Trubitsin, A. V., Bondarenko, I. N., & Sinenko, V. D. (1976). Superconducting Resonance System in Precise Measuring Units. *Cryogenics*, Vol. 16, No. 9, (September 1976), pp. (519-520), ISSN 0011-2275
- Vinet, M., Chapelier, C., & Lefloch, F. (2001). Spatially Resolved Spectroscopy on Superconducting Proximity Nanostructures. *Physical Review B*, Vol. 63, No. 16, (April, 2001), pp. (165420), ISSN 1098-0121
- Vodolazov, D. Y. (2007). Negative Magnetoresistance and Phase Slip Process in Superconducting Nanowires. *Physical Review B*, Vol. 75, No. 18, (May, 2007), pp. (184517), ISSN 1098-0121
- Wagner, R. S., & Ellis, W. C. (1964). Vapor-Liquid-Solid Mechanism of Single Crystal Growth. *Applied Physics Letters*, Vol. 4, No. 5, (March, 1964), pp. (89-90), ISSN 0003-6951
- Wang, J., Ma, X. C., Qi, Y., Fu, Y. S., Ji, S. H., Lu, L., Jia, J. F. & Xue, Q. K. (2007). Negative Magnetoresistance in Fractal Pb Thin Films on Si(111). *Applied Physics Letters*, Vol. 80, No. 11, (March, 2007), pp. (113109), ISSN 0003-6951
- Wang, J., Ma, X. C., Lu, L., Jin, A. Z., Gu, C. Z., Xie, X. C., Jia, J. F., Chen, X. & Xue, Q. K. (2008a). Anomalous Magnetoresistance Oscillations and Enhanced Superconductivity in Single-crystal Pb Nanobelts. *Applied Physics Letters*, Vol. 92, No. 23, (June, 2008), pp. (233119), ISSN 0003-6951
- Wang, J., Ma, X. C., Qi, Y., Fu, Y. S., Ji, S. H., Lu, L., Xie, X. C., Jia, J. F., Chen, X., & Xue, Q. K. (2008b). An Unusual Magnetoresistance effect in the Heterojunction Structure of an Ultrathin Single-crystal Pb film on Silicon Substrate. *Nanotechnology*, Vol. 19, No. 47, (November, 2008), pp. (475708), ISSN 0957-4484

- Wang, J., Shi, C. T., Tian, M. L., Zhang, Q., Kumar, N., Jain, J. K., Mallouk, T. E., & Chan, M. H. W. (2009a). Proximity-Induced Superconductivity in Nanowires: Minigap State and Differential Magnetoresistance Oscillations. *Physical Review Letters*, Vol. 102, No. 24, (June, 2009), pp. (247003), ISSN 0031-9007
- Wang, J., Ma, X. C., Qi, Y., Ji, S. H., Fu, Y. S., Lu, L., Jin, A. Z., Gu, C. Z., Xie, X. C., Tian, M. L., Jia, J. F. & Xue, Q. K. (2009b). Dissipation in an Ultrathin Superconducting Single-crystal Pb Nanobridge. *Journal of Applied Physics*, Vol. 106, No. 3, (August 2009), pp. (034301), ISSN 0021-8979
- Wang, J., Ma, X. C., Ji, S. H., Qi, Y., Fu, Y. S., Jin, A. Z., Lu, L., Gu, C. Z., Xie, X. C., Tian, M. L., Jia, J. F. & Xue, Q. K. (2009c). Magnetoresistance Oscillations of Ultrathin Pb Bridges. *Nano Research*, Vol. 2, No. 9, (September 2009), pp. (671-67), ISSN 1998-0124
- Wang, J., Singh, M., Tian, M., Kumar, N., Liu, B. Z., Shi, C., Jain, J. K., Samarth, N., Mallouk, T. E., & Chan, M. H. W. (2010a). Interplay between Superconductivity and Ferromagnetism in Crystalline Nanowires. *Nature Physics*, Vol. 6, No. 5, (May 2010), pp. (389-394), ISSN 1745-2473
- Wang, J., Jia, J. F., Ma, X. C., Shen, Q. T., Han, T. Z., Jin, A. Z., Lu, L., Gu, C. Z., Tian, M. L., Xie, X. C., & Xue, Q. K. (2010b). Semiconductor-superconductor Transition and Magnetoresistance Terraces in an Ultrathin Superconducting Pb Nanobridge. *Journal of Vacuum Science and Technology*, Vol. 28, No. 4, (July 2010), pp. (678-681), ISSN 1071-1023
- Wolf, S. A., Awschalom, D. D., Buhrman, R. A., Daughton, J. M., von Molnar, S., Roukes, M. L., Chtchelkanova, A. Y., & Treger, D. M. (2001). Spintronics: A Spin-based Electronics Vision for the Future. *Science*, Vol. 294, No. 5546, (November 2001), pp. (1488-1495), ISSN 0036-8075
- Xiong, P., Herzog, A. V., & Dynes, R. C. (1997). Negative Magnetoresistance in Homogeneous Amorphous Superconducting Pb wires. *Physical Review Letters*, Vol. 78, No. 5, (February 1997), pp. (927-930), ISSN 0031-9007
- Yang, Y., Kung, S. C., Taggart, D. K., Xiang, C., Yang, F., Brown, M. A., Guell, A. G., Kruse, T. J., Hemminger, J. C., & Penner, R. M. (2008). Synthesis of PbTe Nanowire Arrays Using Lithographically Patterned Nanowire Electrodeposition. *Nano Letters*, Vol. 8, No. 8, (August, 2008), pp. (2447-2451), ISSN 1530-6984
- Zhang, T., Cheng, P., Li, W. J., Sun, Y. J., Wang, G., Zhu, X. G., He, K., Wang, L. L., Ma, X. C., Chen, X., Wang, Y. Y., Liu, Y., Lin, H. Q., Jia, J. F., & Xue, Q. K. (2010). Superconductivity in One-atomic-layer Metal Films Grown on Si(111). *Nature Physics*, Vol. 6, No. 2, (February, 2010), pp. (104-108), ISSN 1745-2473
- Zhang, Y. F., Jia, J. F., Han, T. Z., Tang, Z., Shen, Q. T., Guo, Y., Qiu, Z. Q., & Xue, Q. K. (2005). Band Structure and Oscillatory Electron-phonon Coupling of Pb Thin Films Determined by Atomic-layer-resolved Quantum-well States. *Physical Review Letters*, Vol. 95, No. 9, (August, 2005), pp. (096802), ISSN 0031-9007



Superconductors - Properties, Technology, and Applications

Edited by Dr. Yury Grigorashvili

ISBN 978-953-51-0545-9

Hard cover, 436 pages

Publisher InTech

Published online 20, April, 2012

Published in print edition April, 2012

Book "Superconductors - Properties, Technology, and Applications" gives an overview of major problems encountered in this field of study. Most of the material presented in this book is the result of authors' own research that has been carried out over a long period of time. A number of chapters thoroughly describe the fundamental electrical and structural properties of the superconductors as well as the methods researching those properties. The sourcebook comprehensively covers the advanced techniques and concepts of superconductivity. It's intended for a wide range of readers.

How to reference

In order to correctly reference this scholarly work, feel free to copy and paste the following:

Meenakshi Singh, Yi Sun and Jian Wang (2012). Superconductivity in Nanoscale Systems, Superconductors - Properties, Technology, and Applications, Dr. Yury Grigorashvili (Ed.), ISBN: 978-953-51-0545-9, InTech, Available from: <http://www.intechopen.com/books/superconductors-properties-technology-and-applications/superconductivity-in-nanoscale-systems>

INTECH
open science | open minds

InTech Europe

University Campus STeP Ri
Slavka Krautzeka 83/A
51000 Rijeka, Croatia
Phone: +385 (51) 770 447
Fax: +385 (51) 686 166
www.intechopen.com

InTech China

Unit 405, Office Block, Hotel Equatorial Shanghai
No.65, Yan An Road (West), Shanghai, 200040, China
中国上海市延安西路65号上海国际贵都大饭店办公楼405单元
Phone: +86-21-62489820
Fax: +86-21-62489821

© 2012 The Author(s). Licensee IntechOpen. This is an open access article distributed under the terms of the [Creative Commons Attribution 3.0 License](#), which permits unrestricted use, distribution, and reproduction in any medium, provided the original work is properly cited.

IntechOpen

IntechOpen